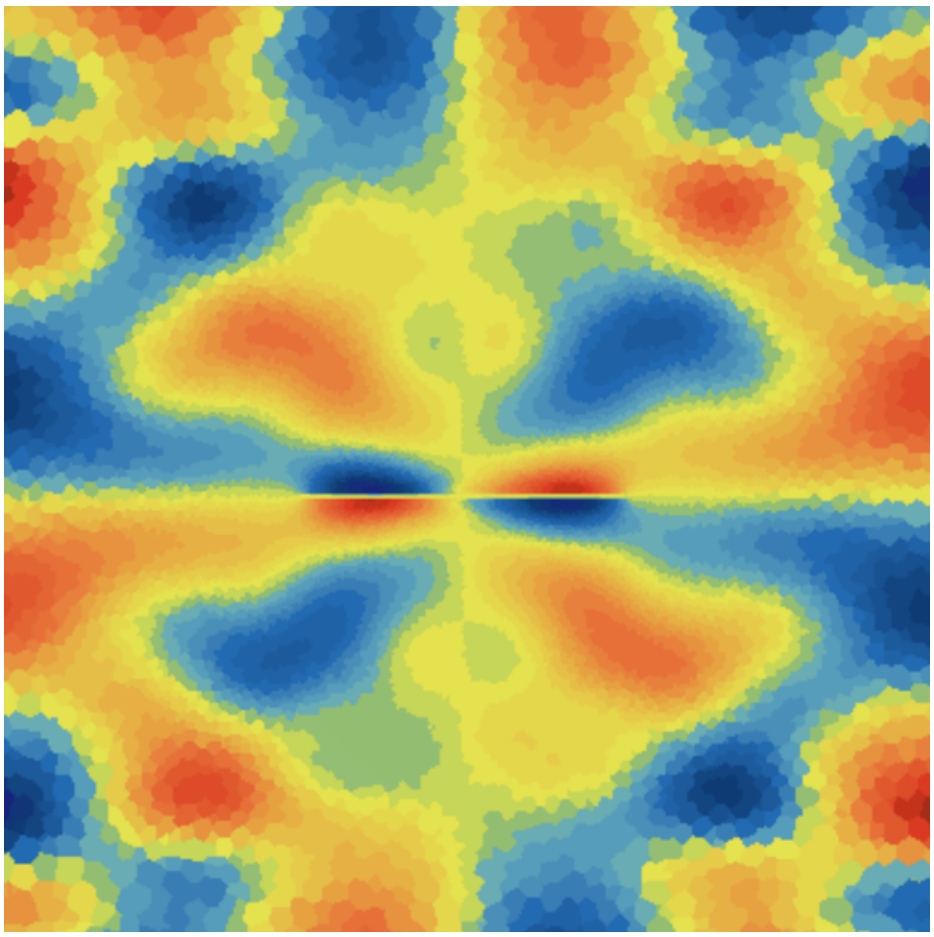

Dynamic Analysis of Submerged Structures

Investigation of added mass, acoustic finite elements and computational fluid dynamics

Master thesis in applied mechanics

HAMPUS PETERSSON

DEPARTMENT OF INDUSTRIAL AND MATERIAL SCIENCES

CHALMERS UNIVERSITY OF TECHNOLOGY
Gothenburg, Sweden 2023
www.chalmers.se

Masters thesis

Dynamic analysis of submerged structures

Investigation of added mass, acoustic finite elements and computational fluid dynamics

Master thesis in applied mechanics

HAMPUS PETERSSON

CHALMERS
UNIVERSITY OF TECHNOLOGY

Department of industrial and material sciences
CHALMERS UNIVERSITY OF TECHNOLOGY
Gothenburg 2023

Dynamic Analysis of Submerged Structures
Investigation of added mass, acoustic finite elements and computational fluid dynamics

Master thesis in applied mechanics

Department of industrial and material sciences
Chalmers University of Technology, 2023

Supervisors:
Stefan Bröyn, FS-Dynamics Sweden AB
Stewart Whitworth, FS-Dynamics Sweden AB
Examiner:
Martin Fagerström, Chalmers University of Technology

Chalmers University of Technology
412 96 Gothenburg
Sweden
Telephone: +46 31 772 1000

Cover page:
Pressure field from CFD-simulation of a submerged, vibrating plate.
Written in LaTeX
Department of industrial and material sciences
Gothenburg 2023

Dynamic analysis of submerged structures
Master thesis in applied mechanics
HAMPUS PETERSSON
Department of industrial and material sciences
Chalmers University of Technology

Abstract

There are a wide range of situations where a structural component is in contact with or submerged in water. Offshore wind turbines, ship hulls, or components in nuclear reactor pools are examples of such structures. Being able to understand and model the behavior of these structures is of great interest. The behavior of a submerged structure can be drastically different from its behavior in air. When comparing the dynamic response of a structure in air and in water, the main effects of submersion are increased damping and decreased eigenfrequency. Added mass and added damping (AMAD) are well-known concepts that are widely used in the analysis of submerged structures. These concepts are used to emulate the interaction between a structure and surrounding water. Analytical expressions for the added mass of simple geometrical shapes undergoing rigid body translation in a fluid have been derived and can be found in design norms e.g. ASME N-1311. These analytical expressions are often applied in an approximate manner to more complex structures for simplicity. Approximate values of damping, based on experiments, can be found in design norms for different types of general structures.

The AMAD model is a computationally effective way of emulating the effects of submersion. Other methods for simulating fluid-structure interaction effects include the use of acoustic finite elements and coupled CFD (computational fluid dynamics) and FE (finite element) solvers. The viability and performance of these three methods have been evaluated in this thesis. The purpose was to investigate alternative and more accurate modeling techniques for the dynamic analysis of submerged structures. The dynamic behavior of a simple geometry was analyzed using the different methods. The results were compared to experimental data for validation. Acoustic finite elements and coupled CFD-FEM have proven to be accurate alternatives to AMAD that could be used more in future work. However, the increased computational cost and complexity of the alternative models call for careful consideration when deciding to use them.

Contents

Preface

This is a master thesis in Applied Mechanics at the department of industrial and material sciences, conducted during the spring of 2023 at the consultancy firm FS-Dynamics. This thesis was made possible thanks to supervisors and future colleagues at FS Dynamics and Professor Martin Fagerström at Chalmers University of Technology. I would like to especially thank Stefan Bröyn, Magnus Ohlson, Stewart Whitworth, and Jakob Dias dos Santos for their time and support during this thesis. I have gained a deeper knowledge and understanding of dynamic analysis using acoustic finite elements and computational fluid dynamics. It has given me valuable insight into the dynamic behavior of submerged structures and the common engineering practices currently used to analyze them. Hampus Petersson
Gothenburg, 2023

Keywords

FEM - Finite element method

CFD - Computational fluid dynamics

Added mass - Method of adding extra mass to a structure to simulate the dynamic effects of fluid-structure coupling.

Added damping - Method of adding damping to a structure to simulate the damping effects a fluid has on a structure moving through it.

FSI - Fluid structure interaction

Acoustic elements - A type of pressure based finite element that can be used for FSI applications.

FFT - Fast fourier transform is an algorithm used to analyse the frequency of input signals.

Ansys - Commercial FE-software.

Abaqus - Commercial FE-software.

Star CCM+ - Commercial CFD software

Notations

l = length

w = width

t = thickness

ρ= density

ζ = damping factor

δ = damping ratio

ω = frequency

ν = Poissons ratio

E = Young's Modulus

c = speed of sound

1 Introduction

1.1 Background

Added mass and added damping (AMAD) are parameters used to model the effect of a structure being submerged in fluid. The effects of submersion are mainly lower eigenfrequencies and higher energy dissipation compared to structures in air. For low-density fluids, these effects are often negligible. When analyzing structures submerged in water, added damping and added mass are parameters that have a significant influence on the results. In design codes, such as ASME N-1311, formulas are presented to calculate added mass for simple geometrical shapes (ASME, 2021). When analyzing more complex structures, the shape of the object is often approximated, like in Figure 1, in a conservative manner with the help of these formulas. Structural damping applied to submerged structures is specified in the code (U.S. Nuclear Regulatory Commission, 2007). A more accurate way of emulating submersion effects is needed to perform more accurate analyses. More precise analysis methods could be used as an alternative to AMAD and as new ways of determining the added mass and damping of more complex geometries.

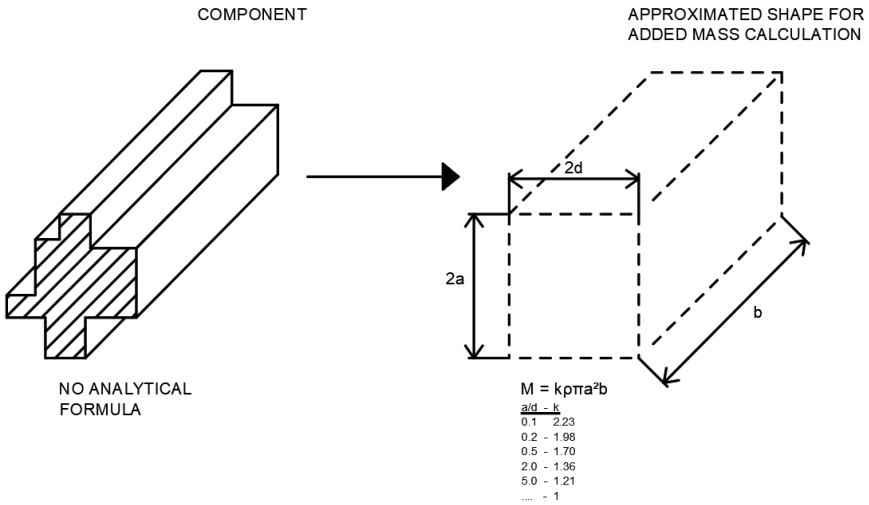

Figure 1: *Example of how a complex-shaped object is approximated into a simpler geometry for calculating its added mass analytically*

As of now, AMAD is often conservatively approximated by assigning parameters valid for simple geometric shapes to the often more complex geometry of the real structure. This conservatism can lead to an overestimation of the stresses in a structure, which for instance can lead to unnecessary repairs. Despite its potential drawbacks in accuracy, there are situations in which AMAD is the only option. One such application is structural analysis with spectral response. Spectral response is a widely used method for seismic analysis of structures that is favored by many because of its simplicity compared to transient analysis (Datta, 2010). A problem with more complex analyses, such as CFD-FEM coupling (Fluid solid interaction-FSI) or acoustic elements when analysing seismic activity is that they are not compatible with spectral response. Spectral response is strictly applicable to linear analysis.

1.2 Purpose

The purpose of this thesis was to investigate different methods for analysing submerged vibrating structures. The concept of added mass, as it is formulated in ASME N-1311, was evaluated and compared to alternative methods. The alternative methods were acoustic finite element modeling and full FSI. The viability and performance of the three modelling techniques was evaluated to find potential advantages or shortcomings

of using the models in different situations. For certain analysis types, the acoustic and FSI analyses could potentially be used as an alternative to AMAD.

In addition, the ability to more accurately determine a structures AMAD using acoustic and full FSI analysis was of interest to investigate. Since one is required to use the AMAD model in certain situations, e.g., spectral response, more accurate approximations of AMAD obtained from the acoustic or FSI models could thereby be an advantage.

1.3 Limitations

To be able to complete the project within the intended time span of the thesis work, a number of limitations had to be set. The complexity of certain aspects within the project had to be reduced in order to produce conclusive results before the deadline. In the following list, the limitations on the project are defined:

1. **Geometrical limitations** - To be able to compare results to the norm guidelines, the analysis was limited to a simple geometry. A flat, rectangular plate, with two different boundary conditions was analysed.
2. **Experimental limitation** - The project was limited to purely numerical analysis and no prototypes or physical tests were produced. Validation against real world observations relied solely on comparisons with experimental data found in the literature.
3. **Material non-linearity** - For the purpose of calculating added mass and added damping, only linear material models were used.
4. **Interaction** - The geometry that was analysed was treated as an "isolated member" in the fluid. There was no interaction with adjacent objects or boundaries taken into consideration.

1.4 Method

In the following subsections, an overview of the structure and workflow of this thesis is described. The first step was to find information on how AMAD has been determined in the "best practice" sense. Analytical solutions, physical experiments and numerical models was studied. After sufficient knowledge was acquired on the different methods of analysis (Added mass, Acoustic elements and FSI), they were applied to a simple structure as a way of analysing their viability in the context of the intended usage.

1.4.1 Literature studies

The first step on the way towards the goal was to gain background knowledge through a literature study. This served the purpose of understanding the problem at hand, what work had been previously done on the subject, and what the different problem areas were. This was done by reading previous books, research papers, and reports on the subject, and taking notes on the relevant information for the project's goals. The main objectives of the literature study were to find experimental data to validate against and establish what had previously been done in the field of research.

1.4.2 Numerical analysis

To analyze the problem at hand, three different analysis methods were applied to simple geometries. This allowed for the comparison of results between the different approaches and for reflecting on their viability with respect to time, computational cost, and precision. The numerical analysis was applied to a simple geometry with two different boundary conditions and was carried out in the following steps:

a) Set up a finite element model of a structure with no damping or added mass. This was to have a reference of the structural behaviour without the effects of submersion.

b) The second step was to model the same structure, applying AMAD according to the norm formulas for the fluid-structure interaction behaviour. The added mass was applied to the model by increasing the density. The added damping was applied in the form of Rayleigh damping.

c) The next step was to model the same structure, but instead of using AMAD, acoustic elements were modelled around the solid to emulate the fluid effects. The structural response was analyzed and used to calculate the added mass and damping effect of the acoustic elements.

d) The final modelling step was to set up a full FSI model of the system, coupling CFD and FEM solvers together. The structural response was analysed and used to calculate the added mass and damping effect of the simulated fluid.

1.4.3 Software

During this thesis, a number of different software packages were used:

Pre-processing
In the case of the AMAD and Acoustic element analyses, all the pre-processing was done in the finite element software Ansys Mechanical. To set up a model in this software, including the definition of geometry, discretization, boundary conditions, material parameters, etc., APDL (Ansys Parametric Design Language) was used. The finite element software used for the full FSI analysis was Abaqus. When using Abaqus for the CFD-coupled simulations, the pre-processing was done using ANSA.

FE-solvers
The FE softwares used for computations in the solid and acoustic domain were Ansys and Abaqus. Ansys was used to perform the AMAD and Acoustic element analyses. For the CFD-coupled analysis, Abaqus was used as the FE solver for the solid domain.

CFD software
The software used for the CFD simulations was STAR-CCM+. This software was chosen in combination with Abaqus for its built-in functions for fluid-structure interaction. The interaction, or data transfer of displacement and pressure fields, was managed via these built in functions.

Post-processing
The results were primarily analyzed using META. To perform calculations on the post processed data, such as a Fast Fourier Transform (FFT), Microsoft Excel was used.

2 Theoretical background

In the following subsections, different methods for describing the effects of fluid-structure interaction are investigated. Previous examples of experiments, simulations, and analytical calculations are discussed to provide sufficient background information on the problem at hand. The chapter aims to provide information on the current state of research in the field of submerged structures and to describe the current methods used in the design of submerged nuclear components.

2.1 Norms for design of nuclear components

When designing nuclear components, regulations mandate that the component meet the requirements of governing codes. The response of structures during stipulated earthquakes are often analysed with dynamic loading. Article N-1000 in the ASME norms, which treatises dynamic analysis methods, is used to analyze such structures (ASME, 2021). The article describes, among other things, how the effects of viscous damping and the concept of added mass can be applied.

2.2 Added mass concept

Added mass is a method used to emulate the fluid-structure coupling forces that occur when a structure is moving through a non-flowing fluid. The method implies that the mass of the structure is increased to emulate the observed effect of decreasing eigenfrequency. The added mass model, as described in the code, depends on the density of the fluid and the shape of the object moving through it. The added mass equations in Table N-1311-1 are stated for 2D cross sections and rigid bodies undergoing 1D translations (ASME, 2021). The equations are determined from the analytical solution of inviscid potential flow with a moving structural boundary. In inviscid potential flow theory, the fluid flow is assumed to be frictionless and non-rotating (Techet, 2005).

The theory is based on the added force that occurs when an object is accelerated in a fluid compared to in a vacuum. The additional force acts in the direction of acceleration, and since mass multiplied by acceleration equals force, the effects of the fluid can be described as an imaginary added mass. An example of how the added mass is derived for a cylinder using potential flow theory can be seen below:

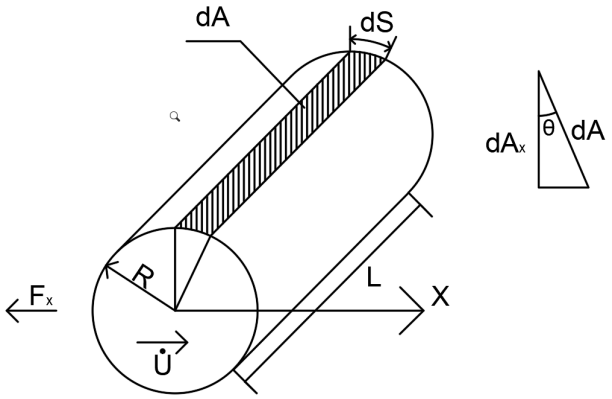

Figure 2: *Rigid cylinder translating in the X-direction.*

Consider the acceleration of a cylinder in the x-direction:

$$\frac{\partial U}{\partial t} = \dot{U} \tag{1}$$

The force acting on the cylinder is obtained by integrating the pressure over the projection of the object's area onto the x-plane.

$$\vec{F_x} = \int P \mathrm{d}\vec{A_x} \tag{2}$$

where: $\mathrm{d}\vec{A_x} = cos(\theta)\mathrm{d}A, \quad \mathrm{d}A = L\mathrm{d}S, \quad \mathrm{d}S = R\mathrm{d}\theta$. R is the radius and L is the length. From unsteady Bernoulli's equation, the expression pressure, P becomes:

$$P = -\rho[\frac{\partial \phi}{\partial t} + \frac{1}{2} \mid \vec{\nabla}\phi \mid^2]. \tag{3}$$

For flow around a cylinder, ϕ becomes:

$$\phi = U\frac{R^2}{r}cos(\theta). \tag{4}$$

With this expression for ϕ, the first term in P becomes:

$$\frac{\partial \phi}{\partial t} \mid_{r=R} = \dot{U}\frac{R^2}{r}cos(\theta) = \dot{U}Rcos(\theta). \tag{5}$$

The second term becomes:

$$\frac{1}{2} \mid \vec{\nabla}\phi \mid^2 \mid_{r=R} = \frac{1}{2} \mid -U\frac{R^2}{r^2}cos(\theta) - U\frac{R^2}{r^2}sin(\theta) \mid^2 = \frac{1}{2}U^2. \tag{6}$$

The force acting on the cylinder is thereby:

$$\begin{aligned} F_x = \int_0^{2\pi} [-\rho[\frac{\partial \phi}{\partial t} + \frac{1}{2} \mid \vec{\nabla}\phi \mid^2]] = \int_0^{2\pi} [-\rho[\dot{U}Rcos(\theta) + \frac{1}{2}U^2]]cos(\theta)RL\mathrm{d}\theta = \\ = -\dot{U}R\int_0^{2\pi} cos^2(\theta)\mathrm{d}\theta - \frac{1}{2}U^2\int_0^{2\pi} cos(\theta)\mathrm{d}\theta = -\rho\pi R^2 L\dot{U}. \end{aligned} \tag{7}$$

The negative sign indicates that the force acts in the direction opposite to the acceleration. This means that the body must resist this force in the positive direction. The added mass can be solved by dividing the force with the acceleration and changing sign (Epps, 2005):

$$M_{added} = \rho\pi R^2 L \tag{8}$$

This expression for the added mass of a rigid cylinder undergoing translations in 2D space is stated in ASME table N-1311-1, along with expressions for a range of other simple geometries. There are also multiple references to analytical expressions for the added mass of shapes not covered by the table. One such reference is "A Design Guide for Calculating Hydrodynamic Mass of Circular Cylindrical Structures" written by S.S. Chen and Ho Chung (S.S Chen & Ho Chung, 1976). This report covers analytical expressions for cylinders vibrating near rigid walls, cylinders with a fluid-filled annulus, motion of cylindrical shells, parallel and eccentric cylinders, and more. Advanced analytical expressions for added mass in 2D motion, taking adjacent objects into account, have proved to be accurate for large wavelengths (S.S Chen & Ho Chung, 1976). However, when the wavelength becomes comparable with the dimensions of the object, as in the case of thin shells, the added mass becomes dependent on the mode shape.

For thin plates, where the flexible motion has a significant effect on the added mass, more involved models have been developed. In a report published in 2007, a mathematical model based on a combination of Sanders shell theory and the finite element method is presented (Y. Kerboua et al., 2007). The model is used to calculate the first five eigenfrequencies of a cantilever plate fully submerged in water. The model gave eigenfrequency results deviating less than 10% from experimental data.

2.3 Added damping according to ASME N-1311

In the design norm N-1311, damping is described as a phenomenon of energy dissipation caused by movement of a structural system (ASME, 2021). The difficulty of analytically determining an accurate damping of a complex structure is addressed with a suggestion of conservative simplified damping models. Values of modal damping, given in percent of critical damping, are presented for a few generalized structures. The damping values lie in the range of 2-7%.

To incorporate viscous damping in a model, the norm presents mass and stiffness proportional damping, also called Rayleigh damping, as an option. To accurately determine the viscous damping matrix of a system, the norm states that experimental data is usually required. This uncertainty regarding fluid damping results in no damping effects from the fluid being taken into account in practice when modeling nuclear components

2.4 Rayleigh Damping

To simulate the damping effect of the water in numerical models, Rayleigh damping is often used. Rayleigh damping is a procedure for determining the generalized viscous damping matrix $\mathbf{C}$ using a linear combination of the mass and stiffness matrices. The formulation for Rayleigh damping can be seen below (Craig & Kurdila, 2006):

$$\mathbf{C} = a_0\mathbf{M} + a_1\mathbf{K}. \tag{9}$$

The constants a_0 and a_1 can be determined to give specific modal damping for two specified modes of interest. To do so, first the damping matrix is diagonalized using the modal matrix, Φ.

$$\mathbf{C} = \Phi^T\mathbf{C}\Phi = diag(C_r) = diag(a_0 + a_1\omega_r^2)M_r = diag(2\zeta_r\omega_r M_r). \tag{10}$$

The same procedure is done for the mass matrix

$$\mathbf{M} = \Phi^T\mathbf{M}\Phi = diag(M_r) \tag{11}$$

and for the stiffness matrix

$$\mathbf{K} = \Phi^T\mathbf{K}\Phi = diag(K_r) = diag(\omega_r^2 M_r). \tag{12}$$

The coefficients a_0 and a_1 can be solved for certain modal damping factor for two specific modes r an s, or rather frequencies ω_r and ω_s, of interest from the following equations:

$$\zeta_r = \frac{1}{2}(\frac{a_0}{\omega_r} + a_1\omega_r). \tag{13}$$

$$\zeta_s = \frac{1}{2}(\frac{a_0}{\omega_s} + a_1\omega_s). \tag{14}$$

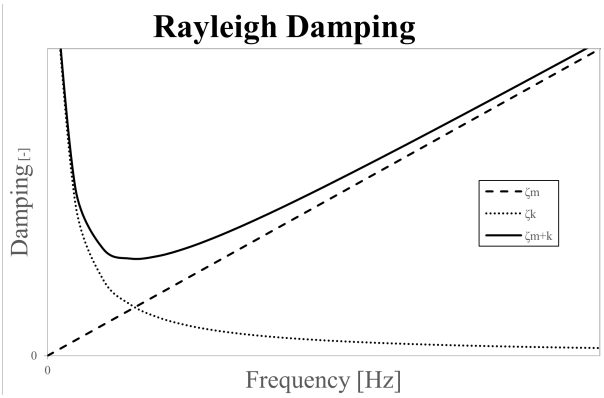

Figure 3: *The graph illustrates the level of Rayleigh damping depending on frequency. The total damping ζ_r, is a linear combination of the mass matrix and the stiffness matrix. The individual damping contributions ζ_m and ζ_k, from the mass and stiffness matrices are plotted. ($\zeta_r = \zeta_m + \zeta_k$)*

2.5 Finite elements

The finite element method is a numerical method used to solve general differential equations approximately (Ottosen & Petersson, 1992). The governing differential equations can describe the physical behavior of certain continua, but finding solutions to these equations for continua with complex geometries and boundary conditions can be inconvenient. The basic idea behind the method is to divide the continuum into a finite number of smaller parts or elements. The solution to the differential equation is assumed to be good enough when evaluated within the sub-region defined by the finite element. Fields, such as stress or strain, can be assumed to vary linearly over an element, while they vary non-linearly over the entire domain.

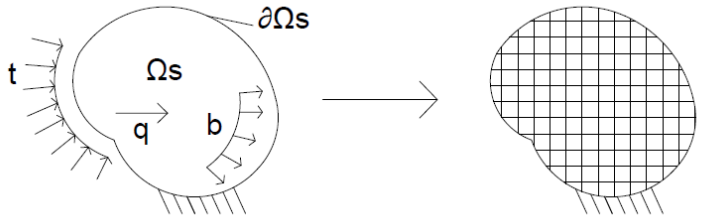

Figure 4: *Arbitrarily shaped solid continua and FE-discretization. Ω_S is the solid domain, $\partial\Omega_S$ is the boundary of the solid domain.*

The solid continua Ω_S in Figure 4 is subjected to a body force $\mathbf{b}$, surface traction $\mathbf{t}$ and an inertia force $\mathbf{q}$. The general differential equation of motion in a 3D solid continuum can be written in Voigt notation as:

$$\bar{\nabla}^T \boldsymbol{\sigma} + \mathbf{b} = \mathbf{q}, \tag{15}$$

where: $\mathbf{q} = \rho \frac{\partial^2 \mathbf{u}}{\partial t^2}$, $\mathbf{u} = \begin{bmatrix} u_1 \\ u_2 \\ u_3 \end{bmatrix}$, $\mathbf{b} = \begin{bmatrix} b_1 \\ b_2 \\ b_3 \end{bmatrix}$.

The vector $\mathbf{u}$ describes the displacement in all three directions, $\mathbf{q}$ is the inertia force and $\mathbf{b}$ is the body force.

Using x_1, x_2 and x_3 as the orthogonal basis of the coordinate system, the differential operator is written as:

$$\bar{\nabla} = \begin{bmatrix} \frac{\partial}{\partial x_1} & 0 & 0 & \frac{\partial}{\partial x_2} & \frac{\partial}{\partial x_3} & 0 \\ 0 & \frac{\partial}{\partial x_2} & 0 & \frac{\partial}{\partial x_1} & 0 & \frac{\partial}{\partial x_3} \\ 0 & 0 & \frac{\partial}{\partial x_3} & 0 & \frac{\partial}{\partial x_1} & \frac{\partial}{\partial x_2} \end{bmatrix}^T \tag{16}$$

The stress-strain relation for the material in question needs to be defined. The matrix, relating stresses to strains in an elastic, isotropic material is denoted as $\mathbf{D}$.

$$\boldsymbol{\sigma} = \mathbf{D}\boldsymbol{\epsilon} \tag{17}$$

To obtain the finite element formulation of the solid continua described above, the general differential equation is first multiplied with an arbitrary weight function. This enables one to apply the Green-Gauss theorem, which divides the differential equation into a surface traction (or boundary) term, a mass term, a volume load (or body force) term, and a stiffness term. Furthermore, the domain is divided into a finite number of elements, with a given number of nodes. The element nodes have degrees of freedom, which means that they can translate in three directions, x_1, x_2 and x_3. The degrees of freedom are grouped into the vector $\mathbf{a}$.The displacements $\mathbf{u}$ are expressed in terms of the nodal translations, and element shape functions defined in the matrix $\mathbf{N}$.

$$\mathbf{u} = \mathbf{N}\mathbf{a} \tag{18}$$

The strains can now be expressed as:

$$\boldsymbol{\epsilon} = \bar{\nabla}\mathbf{N}\mathbf{a} = \mathbf{B}\mathbf{a} \tag{19}$$

The finite element formulation of the structural domain can now be expressed as:

$$\int_{\Omega_S} \mathbf{N}^T \rho \mathbf{N} \mathrm{d}V \ddot{\mathbf{a}} + \int_{\Omega_S} (\mathbf{B})^T \mathbf{D}\mathbf{B} \mathrm{d}V \mathbf{a} = \int_{\partial\Omega_S} \mathbf{N}^T \mathbf{t} \mathrm{d}S + \int_{\Omega_S} \mathbf{N}^T \mathbf{b} \mathrm{d}V, \tag{20}$$

along with essential boundary conditions.

This expression can be written in terms of global stiffness and mass matrices $\mathbf{K}$ and $\mathbf{M}$, along with the boundary and body load vectors $\mathbf{f}_s$ and $\mathbf{f}_b$:

$$\mathbf{M}\ddot{\mathbf{a}} + \mathbf{K}\mathbf{a} = \mathbf{f}_s + \mathbf{f}_b, \tag{21}$$

where:

$$\mathbf{M} = \int_{\Omega_S} \mathbf{N}^T \rho \mathbf{N} \mathrm{d}V, \tag{22}$$

$$\mathbf{K} = \int_{\Omega_S} (\mathbf{B})^T \mathbf{D}\mathbf{B} \mathrm{d}V, \tag{23}$$

$$\mathbf{f}_s = \int_{\partial\Omega_S} \mathbf{N}^T \mathbf{t} \mathrm{d}S, \tag{24}$$

$$\mathbf{f}_b = \int_{\Omega_S} \mathbf{N}^T \mathbf{b} \mathrm{d}V. \tag{25}$$

$$\tag{26}$$

The finite element formulation above contains a component, $\mathbf{f}_S$, that is strongly related to the next subsection on acoustic finite elements. The interaction between acoustic and solid domain is done via the boundary force vector.

2.6 Acoustic elements

Acoustic finite elements have been used to simulate fluid-structure interaction problems in a number of different application areas, such as cars, buildings, or planes (Davidsson, 2004). The acoustic elements in a 3D domain have four degrees of freedom per node: one for each translation in the x, y, and z directions, respectively, and one for pressure. The degrees of freedom related to translation are only active at a fluid-structure interface. There are three main assumptions regarding the fluid behavior. It is assumed to be:

* Irrotational
* Inviscid
* Undergoing small translations

There are three governing differential equations for the acoustic fluid domain. The continuity Equation (27), the Equation of motion (28) and the constitutive Equation (29).

$$\frac{\partial \rho_F(t)}{\partial t} + \rho_0 \nabla \frac{\partial \mathbf{u}_F(t)}{\partial t} = q_F(t) \tag{27}$$

$$\rho_0 \frac{\partial^2 \mathbf{u}_F(t)}{\partial t^2} + \nabla p_F(t) = 0 \tag{28}$$

$$p_F(t) = c_0^2 \rho_F(t) \tag{29}$$

In these equations, ρ_0 refers to the static density, t is the time variable, and c_0 refers to the speed of sound. The displacement and dynamic pressure are denoted as $\mathbf{u}_F(t)$ and $p_F(t)$, respectively. The mass inflow per unit volume and dynamic density are written as $q_F(t)$ and $\rho_F(t)$. In the finite element approximation, the pressure is approximated by the nodal pressures $\mathbf{p}_F$ and element shape functions $\mathbf{N}_F$.

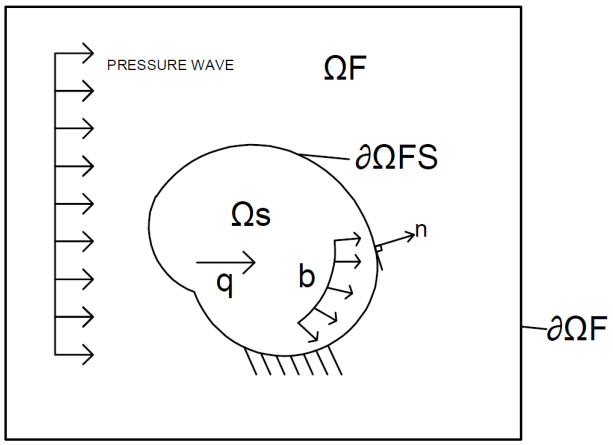

Figure 5: *Solid domain surrounded by acoustic fluid domain. Here, $\partial\Omega_{FS}$ is the boundary shared between the solid and acoustic domain, Ω_F is the acoustic domain, Ω_S is the solid domain, $\partial\Omega_F$ is the outer acoustic boundary, $\boldsymbol{b}$ is the body force, $\boldsymbol{q}$ is the inertia force, and $\boldsymbol{n}$ is the surface normal vector of the solid boundary.*

$$p_F = \mathbf{N}_F \mathbf{p}_F \tag{30}$$

The system of equations is formulated in matrix form as:

$$\mathbf{M}_F\ddot{\mathbf{p}} + \mathbf{K}_F\mathbf{p} = \mathbf{f}_q + \mathbf{f}_S, \tag{31}$$

$$\mathbf{M}_F = \int_{\Omega_F} \mathbf{N}_F^T\mathbf{N}_F dV, \tag{32}$$

$$\mathbf{K}_F = c_0^2 \int_{\Omega_F} ((\nabla\mathbf{N}_F)^T\nabla\mathbf{N}_F dV, \tag{33}$$

$$\mathbf{f}_S = c_0^2 \int_{\partial\Omega_F} \mathbf{N}_F^T\mathbf{n}_F^T\nabla p_F dS, \tag{34}$$

$$\mathbf{f}_q = c_0^2 \int_{\Omega_F} \mathbf{N}_F^T \frac{\partial q}{\partial t} dV. \tag{35}$$

The fluid-structure coupling is based around the motion of the shared boundary between the solid and the fluid. The acceleration normal to the surface determines the pressure on the boundary. The FE-formulation for displacement of the structural boundary $\mathbf{u}_S$ is described by the nodal displacements in the subset, $\mathbf{a}_S$ and the subset of the element shape functions, $\mathbf{N}_S$.

$$\mathbf{u}_S = \mathbf{N}_S\mathbf{a}_S, \tag{36}$$

$$\mathbf{u}_S\mathbf{n} \mid_{\partial\Omega_{SF}} = \mathbf{u}_F\mathbf{n} \mid_{\partial\Omega_{SF}}, \tag{37}$$

where:

$$\mathbf{n} = \mathbf{n}_F = -\mathbf{n}_S, \tag{38}$$

and $\mathbf{u}_F$ is the displacement of the acoustic domain at the boundary $\partial\Omega_{FS}$. The continuity condition for pressure at fluid surface and stress at solid surface is written as:

$$\boldsymbol{\sigma}_S \mid_n = -p_F, \tag{39}$$

where p_F is the acoustic pressure and $\boldsymbol{\sigma}_S$ is the stress at the solid surface. The stress tensor at the structural interface then becomes:

$$\mathbf{S}_S = -p_F \begin{bmatrix} 1 & 0 & 0 \\ 0 & 1 & 0 \\ 0 & 0 & 1 \end{bmatrix}, \tag{40}$$

$$\mathbf{f}_F = \int_{\partial\Omega_{SF}} \mathbf{N}_S^T\mathbf{S}_S\mathbf{n}_S dS = \int_{\partial\Omega_{SF}} \mathbf{N}_S^T\mathbf{n}p_F dS = \int_{\partial\Omega_{SF}} \mathbf{N}_S^T\mathbf{n}\mathbf{N}_F dS\mathbf{p}_F. \tag{41}$$

The fluid force $\mathbf{f}_F$ is acting in the opposite direction to the normal vector of the structural surface. The magnitude is determined by the acoustic nodal pressures $\mathbf{p}_F$. The force exerted by the structure on the fluid is introduced in the term $\mathbf{f}_S$. To express this, Equation (28) is combined with the boundary condition in Equation (37).

$$\mathbf{n}^T\nabla p_F|_{\partial\Omega_{SF}} = -\rho_0\mathbf{n}^T\frac{\partial^2\mathbf{u}_F}{\partial t^2}|_{\partial\Omega_{SF}} = -\rho_0\mathbf{n}^T\frac{\partial^2\mathbf{u}_S}{\partial t^2}|_{\partial\Omega_{SF}} = -\rho_0\mathbf{n}^T\mathbf{N}_S\ddot{\mathbf{a}}_S|_{\partial\Omega_{SF}} \tag{42}$$

The force $\mathbf{f}_S$ on the fluid boundary was expressed in Equation (34), and can now be expressed in terms of structural acceleration.

$$\mathbf{f}_S = -\rho_0 c_0^2 \int_{\partial\Omega_{FS}} \mathbf{N}_F^T\mathbf{n}^T\mathbf{N}_S dS\ddot{\mathbf{a}}_S \tag{43}$$

The force acting on the structure $\mathbf{f}_F$, and the force acting on the fluid $\mathbf{f}_S$ can both be expressed by the spatial coupling matrix $\mathbf{H}_{SF}$.

$$\mathbf{H}_{SF} = \int_{\partial\Omega_{SF}} \mathbf{N}_S^T \mathbf{n} \mathbf{N}_F dS \tag{44}$$

$$\mathbf{f}_F = \mathbf{H}_{SF}\mathbf{p}_F \tag{45}$$

$$\mathbf{f}_S = -\rho_0 c_0^2 \mathbf{H}_{SF}^T \ddot{\mathbf{a}}_S \tag{46}$$

The coupled acoustic-structure system of equations can be expressed as (Davidsson, 2004):

$$\begin{bmatrix} \mathbf{M}_S & \mathbf{0} \\ -\rho_0 c_0^2 \mathbf{H}_{SF}^T & \mathbf{M}_F \end{bmatrix} \begin{bmatrix} \ddot{\mathbf{a}}_S \\ \ddot{\mathbf{p}}_F \end{bmatrix} + \begin{bmatrix} \mathbf{K}_S & -\mathbf{H}_{SF} \\ \mathbf{0} & \mathbf{K}_F \end{bmatrix} \begin{bmatrix} \mathbf{a}_S \\ \mathbf{p}_F \end{bmatrix} = \begin{bmatrix} \mathbf{f}_b \\ \mathbf{f}_q \end{bmatrix} \tag{47}$$

2.7 Computational Fluid Dynamics

Computational fluid dynamics (CFD), with the use of the finite volume method (FVM), is a common way to analyse fluid behavior. Much like in FE-modeling of solid structures, a fluid domain is discretized into a finite number of volume cells. The fundamental laws of fluid mechanics are the conservation of mass, conservation of linear and angular momentum, and conservation of energy (Siemens Digital Industries Software, 2023). Conservation of mass can be described by the continuity equation:

$$\frac{\partial \rho}{\partial t} + \nabla(\rho \mathbf{v}) = 0 \tag{48}$$

Where $\mathbf{v}$ is the velocity and ρ is the density. The conservation of linear and angular momentum is described by the two following equations:

$$\frac{\partial(\rho \mathbf{v})}{\partial t} + \nabla(\rho \mathbf{v} \otimes \mathbf{v}) = \nabla \boldsymbol{\sigma} + \mathbf{f}_B \tag{49}$$

$$\boldsymbol{\sigma} = \boldsymbol{\sigma}^T = -p\mathbf{I} + \mathbf{T} \tag{50}$$

Equation (48) implies that the rate of change of linear momentum equals the resultant force that is acting on the continuum. The resultant of body forces, such as centrifugal or gravitational, is denoted as $\mathbf{f}_B$. The conservation of angular momentum requires the stress tensor $\boldsymbol{\sigma}$ to be symmetric, which is described in Equation (49). The stress tensor can be written as a sum of the normal stress tensor, $-p\mathbf{I}$, and the shear stress tensor, $\mathbf{T}$. The shear stress tensor depends on the fluid viscosity. For incompressible, Newtonian fluids, such as water, the shear stress tensor, $\mathbf{T}$, is related to the strain rate-tensor, $\mathbf{D}$, via a constant dynamic viscosity as:

$$\mathbf{T} = 2\mu\mathbf{D} \tag{51}$$

$$\mathbf{D} = \frac{1}{2}(\nabla \mathbf{v} + (\nabla \mathbf{v})^T) \tag{52}$$

The conservation of energy is described by applying the first law of thermodynamics to the volume. The first law of thermodynamics implies that the change in internal energy of a system is equal to the sum of the total work and the total heat transfer in and out of the system:

$$\frac{\partial(\rho E)}{\partial t} + \nabla(\rho E \mathbf{v}) = \mathbf{f}_B \cdot \mathbf{v} + \nabla(\mathbf{v} \cdot \boldsymbol{\sigma}) - \nabla \mathbf{q}_F + S_E \tag{53}$$

E denotes the energy per unit mass, $\mathbf{q}_F$ is the heat flux and S_E is the energy source per unit volume.

3 Numerical implementation

The main objective of this thesis is to investigate alternative methods to the AMAD model, which is widely used in the current design of submerged structural components. This will be done in a number of steps and for different geometry setups. The analysis will be based on a plate geometry that was experimentally tested with regards to damping and eigenfrequency. The rectangular plate was tested with two different boundary conditions: both clamped and then simply supported along two of its four edges. The AMAD, acoustic, and full FSI models will be applied to the geometry, and the results will be compared against the experimental data.

3.1 Simply supported plate

The first analysis is of a rectangular plate, simply supported at both of its shortest sides. The geometry was modeled based on a plate that was experimentally tested by M. R. Haddara and S. Cao at Memorial University of Newfoundland (M. R. Haddara & S. Cao, 1996). Eigenfrequency, added mass coefficient and damping data was obtained for the first five modes of vibration, which will be used to validate the numerical analysis results. Added mass coefficients and eigenfrequencies for the first five eigenmodes can be seen in Table 1. The added mass factor refers to the ratio between the added mass and the original plate mass.

Table 1: *Plate geometry and material data: l=655 mm; w=201.65 mm; t= 9.36 mm; ν=0.3 [-]; ρ=7850 kg/m^3; E=207 GPa. The added mass factor is calculated using the difference in frequency between water and air according to the formula* $\frac{M_{add}}{M_{plate}} = (\frac{\omega_{air}}{\omega_{fluid}})^2 - 1$

Mode	Frequency submerged in water [Hz]	Frequency in air [Hz]	Added mass factors $\frac{M_{add}}{M_{plate}}$	Type
1	28.723	50.539	2.0959	1st bending
2	117.125	197.737	1.8502	2nd bending
3	154.510	210.933	0.8637	1st torsional
4	281.795	439.654	1.4342	3rd bending
5	335.040	453.976	0.8360	2nd torsional

The experimental data was obtained using a fast sine sweep excitation via a connecting rod placed near the center of the plate. A fast sine sweep excitation implies that an input signal or force is applied as a sine function with gradually increasing frequency. The applied force was monitored via a force transducer placed between the connecting rod and the plate. The response of the plate was measured via 15 accelerometers placed in a grid formation on the plate. The input force signal and the accelerometer data were then fed into an oscilloscope for monitoring, and a dual-channel signal analyzer to perform a fast Fourier transform (FFT). The frequency response could thereby be obtained. The processed data from the dual-channel signal analyzer was then analyzed on a computer running commercial software developed by Structural Measurement Systems.

To emulate a friction-free, "hinged" support at the short ends of the plate, notches were cut to weaken the plate at the supports. Beyond the notches, the plate continued on and was clamped over a distance of 300 mm. This gave the plate hinge-like supports with minimal friction.

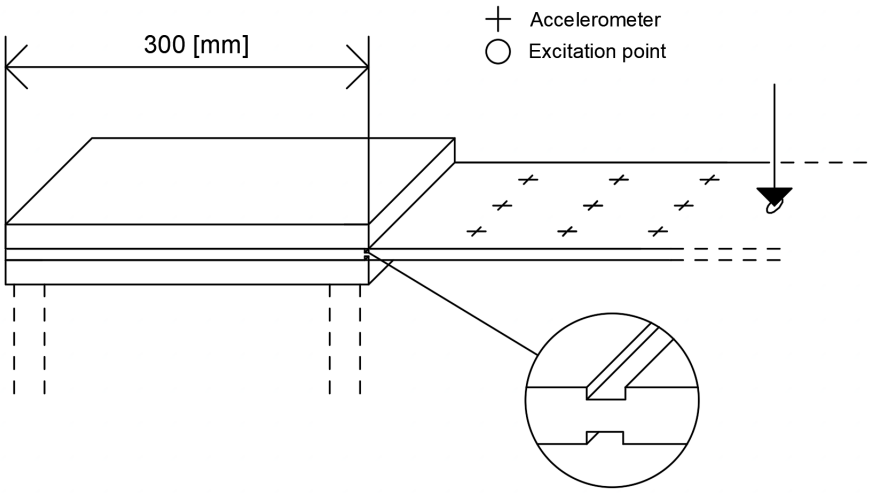

Figure 6: *Schematic illustration of the experimental setup. The placement and number of accelerometer points are only for illustration purposes. The zoomed-in detail drawing illustrates the notches made to emulate a simply supported boundary condition.*

3.2 Partially clamped plate

The second case analyzed is a plate with the same material properties and dimensions as the simply supported plate described in Subsection 3.1, except for the different boundary conditions. In this analysis, the plate had clamped boundary conditions along both its shorter edges. This plate was also experimentally examined by M. R. Haddara and S. Cao (M. R. Haddara & S. Cao, 1996). The relevant data from the experiment can be seen in Table 2 and 3.

Table 2: *Plate geometry and material data: l=655 mm; w=201.65 mm; t= 9.36 mm; ν=0.3 [-]; ρ=7850 kg/m^3; E=207 GPa*

Mode	Frequency in air [Hz]	Type
1	100.081	1st bending
2	244.515	1st torsional
3	279.062	2nd bending
4	517.020	2nd torsional
5	532.138	3rd bending

Table 3: *Table with experimental data containing the frequency in water, and the added mass factors for the partially clamped plate.*

Mode	Frequency in water [Hz]	Added mass factor $\frac{M_{add}}{M_{plate}}$	Type
1	57.444	2.0354	1st bending
2	167.010	1.7920	2nd bending
3	179.152	0.8628	1st torsional
4	344.999	1.3791	3rd bending
5	385.739	0.7965	2nd torsional

The report by Haddara and Cao describes how the "clamped" boundary conditions were applied to the plate in the experiment. The plate was clamped over a distance of 300 mm, continuing beyond the free span at both ends. An illustration of the experimental setup can be seen in Figure 6, with the exception of the notch, which was only used for the simply supported plate. The concept of truly clamped boundary conditions implies that the material at the boundary cannot move, which cannot be achieved in reality. One could note that the mode types changes place in the frequency order when submerged in water for this plate setup.

3.3 Added mass and damping from transient response

The added mass factor refers to the ratio between the added mass, M_{add}, and the mass of the plate, M_{plate}. The added mass, when transitioning from air to water can be determined from the difference in eigenfrequency between the submerged plate, and the plate in air according to the following equation:

$$\omega_{fluid} = \omega_{air} \frac{1}{\sqrt{1 + \frac{M_{add}}{M_{plate}}}} \tag{54}$$

To obtain the added mass for a structure, one must know the initial weight, and the frequencies in air and water, respectively.

The procedure for calculating the damping factor is to take peak values of displacement, y_i and y_{i+1} in a node, for two subsequent oscillatory cycles and apply the following formula (Roger Y. Lu & David D. Seel, 2006):

$$\delta = \ln \frac{y_i}{y_{i+1}} \tag{55}$$

$$\zeta = \frac{\delta}{\sqrt{4\pi^2 + \delta^2}} \tag{56}$$

To obtain the damping, the amplitude was measured at the first and second oscillation peak. This gives the damping in relation to critical damping, i.e. a ζ value of 1 corresponds to critical damping.

3.4 AMAD analysis method

3.4.1 FE-model

The plates were modelled using APDL in Ansys Mechanical, with solid-186 elements, consisting of 20 nodes and 3 translation degrees of freedom (dofs) per node. The discretization was determined in the mesh convergence study found in Subsection 4.1. The solid-186 elements were chosen because of their capability to describe bending without use of rotation dofs. The reason for avoiding rotation dofs is to ensure compatibility with the coupling of the acoustic elements and the CFD-solver later used in the thesis. The same mesh of the solid structure can thereby be used in both the AMAD, Acoustic and CFD-coupled analysis. The boundary conditions were tuned so that the frequency without submersion matched the experimental data as good as possible. To adjust the frequency, the number of fixed nodes was decreased. Instead of constraining all the nodes in the thickness, only the three middle nodes were constrained. The same principle was used for nodes along the plate width, which resulted in only a portion of the nodes being constrained. Figures 7a and 7b illustrate how the boundary conditions were applied. When fully constraining all nodes at the partially clamped, FE-plate ends, the plate model became overly stiff, and the frequency of the FE-model without fluid effects deviated significantly from the experiment in air. To come closer to the true structural behavior in air, the number of clamped nodes was decreased, and only a portion of the plate ends were constrained.

3.4.2 Analysis procedure

The FE-plates were analysed with the AMAD model to emulate the fluid effects. To obtain the results for comparison with experimental data, the procedure described below was followed:

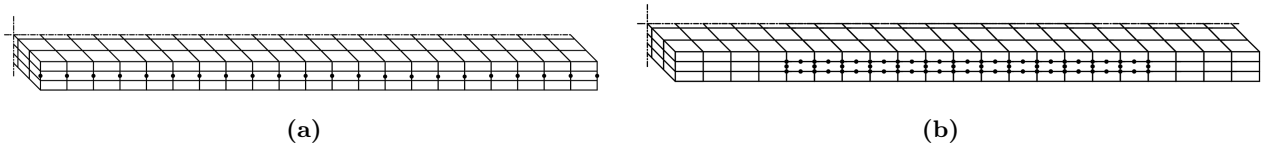

(a) **(b)**

Figure 7: ***a)*** *Boundary condition layout of the simply supported plate, the dots indicate nodes where all translations were locked. This boundary condition was reused in all analysis types,* ***b)*** *Boundary condition layout of the partially clamped plate, the dots indicate nodes where all translations were locked. This boundary condition was reused in all analysis types*

1. A modal analysis of the plates were performed to obtain the mode shapes of the first five eigenmodes.
2. Prescribed displacements were applied in the shapes of those eigenmodes to obtain initial conditions for the transient analysis. The modes were normalized and scaled to get the desired initial amplitude. This was done for one mode at a time.
3. The prescribed displacements were removed at the first time step of the transient analysis to release the structure into free vibration. Rayleigh damping (3%) was assigned according to norms used in current design (U.S. Nuclear Regulatory Commission, 2007). This level of damping refers solely to the structural losses. Damping from the fluid is not taken into account in most cases, to be on the conservative side.
4. Time-displacement data from the node with maximum displacement in each plates discretization was obtained and FFT was used to determine the eigenfrequencies.

When applying a prescribed displacements to the plate that correspond to the shape of the eigenmode of interest, one obtains a frequency response with less noise compared to a more standard "guitar pick" type of pluck test. The modes that are not of interest are not excited as much when the plate is initiated to vibrate in a certain mode shape. This makes it easier to obtain the eigenfrequencies from a transient analysis (W.R. Marcum et al., 2019). When analysing the plate with the AMAD model, one can obtain the eigenfrequency from only running a modal analysis. However, since the FSI model isn't compatible with a simple modal analysis, the transient response is needed for comparison.

The added mass was applied to the finite element model by increasing the density of the plate. To determine the amount of added mass, Table N-1311-1, in the ASME norm was used.

$$M_{add} = k\rho_{water}\pi a^2 b \tag{57}$$

$$\rho_{new} = \frac{M_{plate} + M_{add}}{V_{plate}} \tag{58}$$

Where: $a = \frac{w}{2}$; $b = l$; $d = \frac{t}{2}$; $k = 1$, if $d << a$

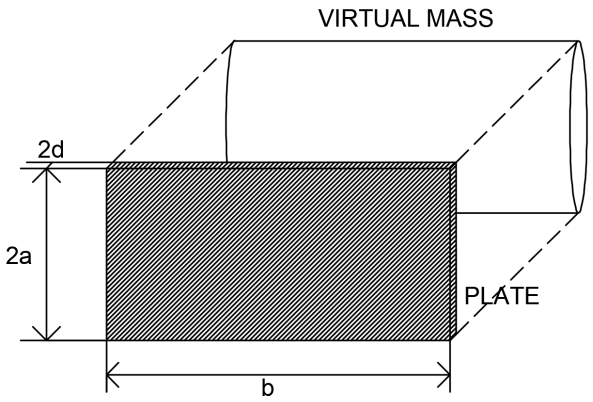

Figure 8: *Illustration of the virtual mass added to the plate*

The added mass was calculated to 20.9078 kg and the plate mass is 9.7048 kg. This gives an added mass factor of 2.1543 [-].

3.5 Acoustic element analysis method

3.5.1 FE-Model

The plates were modelled using solid-186 elements, with the discretization chosen in the mesh convergence study in chapter 4.5. The interaction between solid and acoustic elements was defined on the set of shared nodes between the first acoustic layer and the outermost solid layer. The first layer of the acoustic domain was modelled with fluid-220 elements. This element type was chosen for compatibility reasons, as it has the same geometry and number of nodes as the adjacent solid elements. The section outside of the first layer was modelled with tetrahedral, fluid-30 elements. The lower order fluid-30 elements were chosen for their capacity to describe pressure, whilst keeping a lower computational cost. The outermost layer of fluid elements was modelled with fluid-130 elements in the shape of a sphere. These pressure-only, shell elements have the ability to describe the effects of having an "infinite" fluid domain. The acoustic sphere can be seen in Figure 9a, and the embedded plate in Figure 9b.

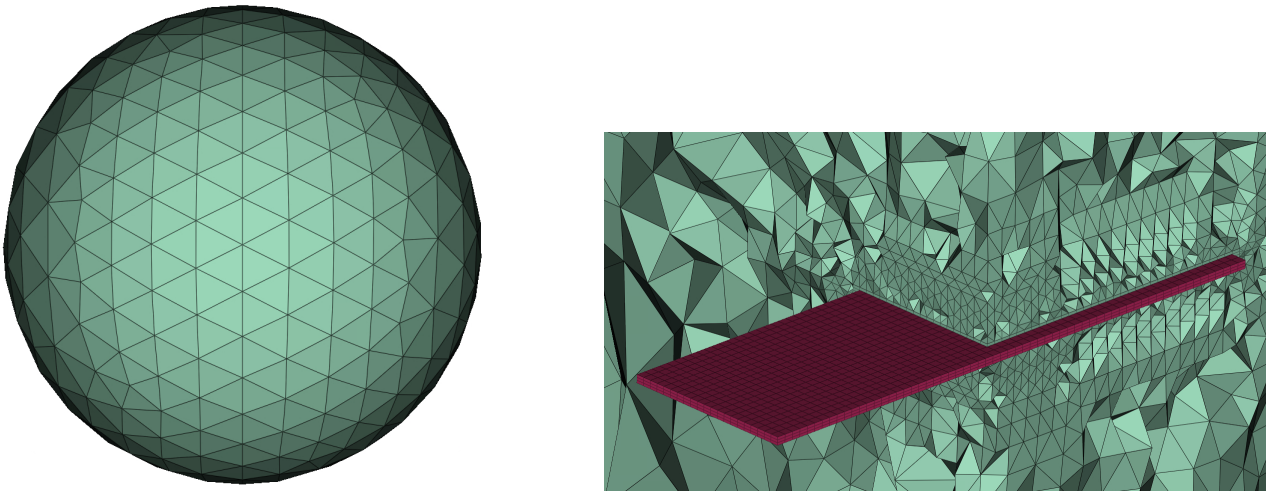

(a) **(b)**

Figure 9: ***a)*** *Illustration of the spherical acoustic domain ,****b)*** *Illustration of the plate within the acoustic sphere.*

3.5.2 Analysis Procedure

The analysis was conducted in the following steps:

1. A modal analysis of the plate was performed to obtain the mode shapes of the first five eigenmodes.
2. Prescribed displacements were applied in the shapes of those eigenmodes to obtain initial conditions for the transient analysis. The modes were normalized and scaled to get the desired initial amplitude. This was done for one mode at a time.
3. The prescribed displacements were removed at the first time step of the transient analysis to release the structure into free vibration.
4. Time-displacement data from the node with maximum displacement in the plate discretization was obtained and FFT was used in combination with period measurements to determine the eigenfrequencies.

To calculate the eigenfrequenies, FFT was applied to the transient displacement data. When analysing the frequency transformed data, one can see if the response has interference from other modes of vibration. If the transform yields a frequency response without interference, only one sharp amplitude peak will appear. The experiment report written by Haddara and Cao states that there was no noticeable difference in mode shape between the experiments in air and water (M. R. Haddara & S. Cao, 1996). The mode shapes obtained from the plate FE-model without fluid effects were therefore assumed to be eligible to use for fluid simulations.

3.6 Full FSI analysis method

3.6.1 FE-Model

For this analysis, the FE-model was coupled to a CFD-model to capture the structure-fluid interaction behaviour. The FE-model of the solid domain remained unchanged in principle. To avoid file based coupling between Ansys and Star-CCM+, the FE-software was changed from Ansys to Abaqus. File based coupling implies that the data transfer of displacements, wall shear stresses and pressures between two software

is managed via third party coupling scripts. Abaqus and Star-CCM+ are more compatible software's for fluid-structure interaction as built in functions are available to manage the data transfer of displacement, wall shear force and pressure. The material properties, boundary conditions and discretization remained identical, and a 20-node solid element (C3D20) was used in Abaqus that corresponds to the solid-186 element in Ansys.To ensure that the results from the FE model differed a negligible amount between Ansys and Abaqus the transient response from the modal loading analysis was compared without fluid effects. The result of this comparison can be seen in Figure 10.

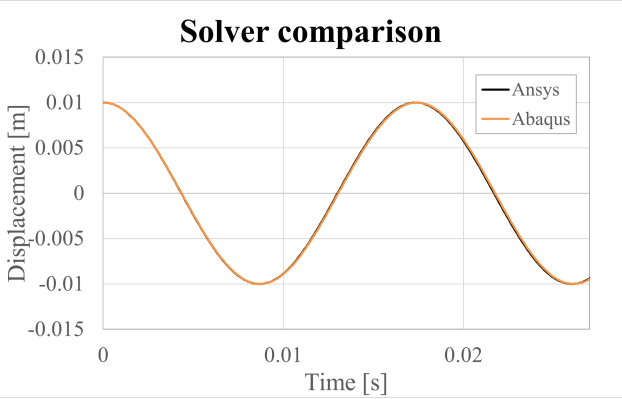

Figure 10: *Comparison of transient response from different FE-solvers*

Figure 10 confirms that there is a negligible difference between the results from the different FE solvers. The difference was determined to be within an acceptable range for continuing seamlessly with the Abaqus solver for producing results.

3.6.2 CFD-Model

The CFD-model domain was set-up as a cubic geometry surrounding the plate. The side length of the cube was initially set to 1 m which proved to be insufficient in order to avoid interaction between the outer boundary and the plate. The size was iterated upon to finally arrive at a side length of 2 m. The discretization of the fluid domain is discussed in detail in the discretization chapter.

The turbulence model selected for this analysis was the SST (Menter) K-Omega model (Siemens Digital Industries Software, 2023). The conservation equations of mass and momentum were solved sequentially using a segregated flow solver. The coupling between Abaqus and Star CCM+ was done explicitly, according to a staggered approach. The incompressibility of water proved to be hard to solve. If a fluid is incompressible, this means that in theory, the speed of sound tends toward infinity. When the plate surfaces translate in the fluid, a pressure wave propagates. The pressure wave has a speed that tends toward infinity, which numerically speaking means that an infinitely small time step is needed to capture it. To circumvent this issue, the incompressibility of the fluid was relaxed. Two field functions were used to describe the density ρ_F and the density derivative $\dot{\rho_F}$. The expressions for density with regards to sonic velocity and pressure comes from 1D compressible flow equations (Anderson, 2003):

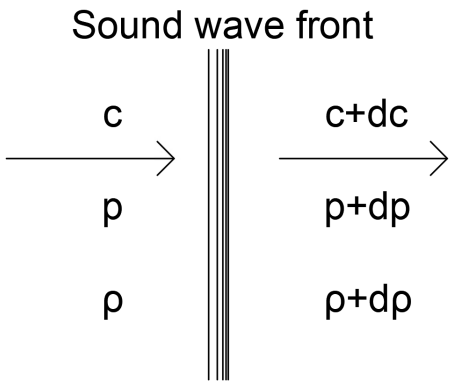

Figure 11: *Schematic illustration of a sound wave. c is the sonic velocity, p is the pressure and ρ is the density*

The flow ahead of the sound wave depicted in Figure 11 moves toward the wave at the velocity c, with a density of ρ_1 and a pressure of p_1. The flow behind the wave moves away from it at the velocity $c + \mathrm{d}a$, with density and pressure equal to $\rho_1 + \mathrm{d}\rho$ and $p_1 + \mathrm{d}p$. The flow through the sound wave is assumed to be one dimensional, and the continuity equation for steady one dimensional flow therefore yields:

$$\rho c = (\rho + \mathrm{d}\rho)(c + \mathrm{d}c) \tag{59}$$

$$\rho c = \rho c + c\mathrm{d}\rho + \rho \mathrm{d}c + \mathrm{d}\rho \mathrm{d}c \tag{60}$$

The term $\mathrm{d}\rho \mathrm{d}c$ is small compared to other terms and can therefore be neglected. This yields:

$$c = -\rho \frac{\mathrm{d}c}{\mathrm{d}\rho} \tag{61}$$

The momentum equation for steady one dimensional flow can also be applied. If, like in Equation (61), the product of differentials are ignored, this yields:

$$\mathrm{d}p = -2c\rho \mathrm{d}c - c^2 \mathrm{d}\rho \tag{62}$$

Equation (62) could now be solved for $\mathrm{d}c$, which was then substituted in Equation (61).

$$c = -\rho \frac{\frac{\mathrm{d}p}{\mathrm{d}\rho} + c^2}{-2c\rho} \tag{63}$$

$$c^2 = \frac{\mathrm{d}p}{\mathrm{d}\rho} \tag{64}$$

The difference in pressure $\mathrm{d}p$, can be expressed as $\mathrm{d}p = p - p_0$, where ρ_0 is the reference pressure. In the application of this thesis, the reference pressure p_0 is zero. The reference density, or static density is denoted ρ_0.

$$c^2 = \frac{p - p_0}{\rho - \rho_0} \tag{65}$$

$$\rho = \rho_0 + \frac{p}{c^2} \tag{66}$$

$$\dot{\rho} = \frac{1}{c^2} \tag{67}$$

Where: p = *Pressure*, ρ_0 = *Static density* and c = *Speed of sound*

The density was described as a function of the pressure and the speed of sound, rather than being set to a constant value (incompressible). A parametric study of the incompressibility was conducted to determine its impact on the results. The parametric study can be seen in the Subsection 4.2. The boundary conditions at the outer surfaces of the fluid domain was set as unsteady, non reflecting pressure outlets. The purpose was to avoid reflections of pressure waves from the boundary's which would interfere with the response.

3.6.3 Fluid structure coupling

The fluid-structure coupling between the solid domain in Abaqus and the fluid domain in Star-CCM+ is done by interchanging displacement, pressure and wall shear stress- fields. The analysis was set up so that Abaqus leads the solution process. This meant that the first time step started with Abaqus computing the nodal displacements of the plate. The displacement field was then sent to Star-CCM+ that computed the fluid solution, containing pressures and shear forces on the plate surface. These fluid pressures and shear forces were then mapped onto the surface nodes of the plate mesh. Abaqus then computed a new displacement field, based on the imported fluid forces. The next time step can then be initiated and the process repeats.

3.6.4 Analysis procedure

The plates were analysed in a similar manor to the Acoustic and AMAD models. The difference was that instead of starting the transient solution with the plate deformed according to the mode shape, the analysis was started from the original plate position. The decision to start from an non-deformed plate was taken to simplify the simulation procedure. To start the analysis with the deformed shape requires additional steps in the model preparation. The analysis was setup in the following steps:

1. A modal analysis of the plate was performed to obtain the first five mode shapes.
2. A prescribed displacement, in the shape of a certain mode, was applied to the plate in a static analysis.
3. The forces at all the nodes in the x,y and z direction were obtained for all mode shapes respectively.
4. A transient analysis with the full fluid solid interaction was initiated and the modal load was slowly ramped up.
5. When the load reached full magnitude, it was kept constant for a time period long enough for the plate to stabilize.
6. After the plate had stabilized, the forces were removed and the plate was released into free vibration.

The transient displacement data of the node with maximal displacement was obtained for all modes and FFT, was used to obtain the frequency.

4 Results

In this chapter, the results from the numerical implementations are presented. The simply supported and partially fixed plates have been analysed with three different numerical methods, AMAD, Acoustic elements and full FSI. In addition, a mesh convergence study has been conducted for the plate and the acoustic element sphere. A parametric study of incompressibility was conducted for the FSI-model and can also be seen in this chapter.

4.1 Discretization

To minimize the computational cost, and to get reliable results, discretization studies were conducted. The goal with these studies were to find discretizations with sufficient accuracy that produced stable results, whilst not using an excessive amount of computational resources.

4.1.1 Plate discretization

To select a discretization that provided sufficient accuracy for the analysis, a mesh convergence study was conducted. The first mesh convergence study involved the simply supported plate geometry, modelled with 20 node solid elements, denoted as Solid-186 in Ansys. The geometry and layout of the Solid-186 element can be seen in Figure 12 The plate was discretized with different mesh sizes and put through a modal analysis. The discretizations were constructed with different aspect ratios and different number of element layers through the thickness of the plate. The aspect ratio refers to the ratio between the elements longest and shortest side. An aspect ratio of 0.5 means that the shortest element side, is half the length of the longest element side. The purpose of this was to define the limits for how to construct the mesh. The plots in Figure 13a and 13b show the relation between the fifth eigenfrequency, aspect ratio and number of elements through the thickness. The results were obtained with 4 significant digits. The fifth eigenmode was the only result that varied with any significance.

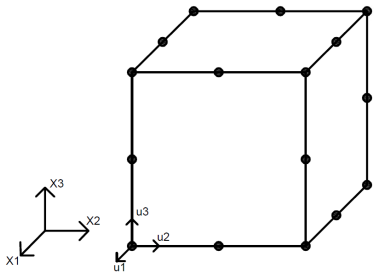

Figure 12: *20 node FE-element with 3 degrees of freedom per node (Solid-186)*

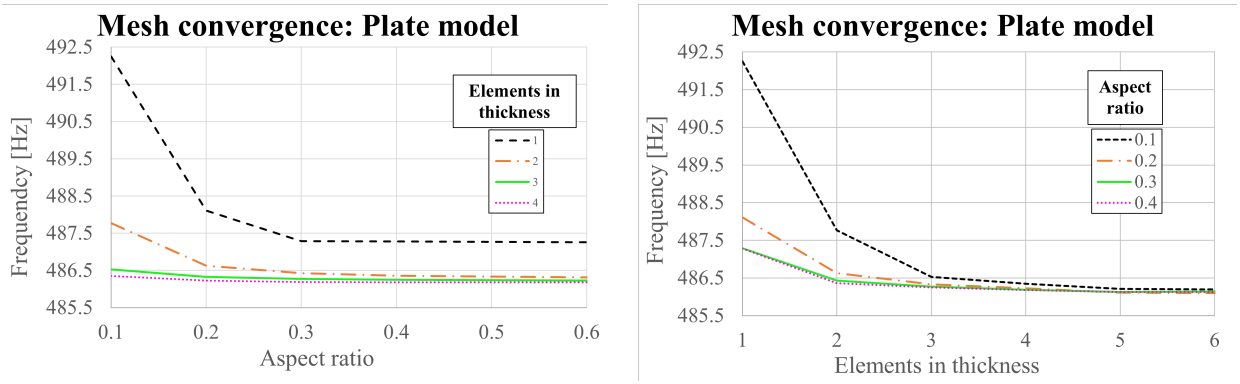

(a) **(b)**

Figure 13: ***a)*** *Convergence plot illustrating the frequency of the second bending mode, depending on aspect ratio. The frequency to aspect ratio is plotted for different number of elements within the plate thickness ,****b)*** *Convergence plot illustrating the frequency of the second bending mode, depending on elements within plate thickness. The frequency to number of elements is plotted for different aspect ratios.*

When analysing the results from the plate-mesh convergence study, one can conclude that the result varies a negligible amount when passing the threshold of three elements over the plate thickness, and an aspect ratio of at least 0.3. The total number of elements and thereby the computational cost increases exponentially when increasing the aspect ratio. To increase the number of elements through the thickness is more computationally effective, as it doesn't require an exponential increase of the total element number.

	0.1	0.2	0.3	0.4	0.6
1	98.76%	99.59%	99.76%	99.76%	99.77%
2	99.66%	99.90%	99.94%	99.95%	99.96%
3	99.92%	99.96%	99.97%	99.98%	99.98%
4	99.95%	99.98%	99.99%	99.99%	99.99%
5	99.98%	100.00%	100.00%	100.00%	100.00%
6	99.99%	100.01%	100.00%	100.00%	100.00%

(a)

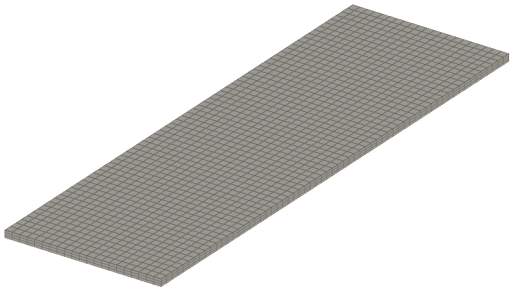

(b)

Figure 14: ***a)*** *Table with frequency values, normalized against the frequency obtained from the finest mesh tested (aspect ratio = 0.6, elements in thickness = 6). The columns represent aspect ratios, and the rows represent the number of elements within the thickness. ,****b)*** *Illustration of the plate discretization used for producing results.*

Figure 14a shows a table over the accuracy of the different discretizations relative to the finest mesh tested. The columns represent different aspect ratios, the rows represent number of elements in the thickness. One can see that all the discretizations deviate less than 2% from the finest one. The red box indicates the discretization that is depicted in Figure 14b. This is the mesh that lie on the threshold of sufficient accuracy, and it was therefore chosen for producing results. The mesh was determined to be sufficiently accurate as it produced frequency results deviating 0.03% from the finest mesh tested, which is within the level of accuracy

needed for producing results. The results were presented in Hz with one decimal point.

4.1.2 Acoustic-fluid discretization

The fluid solid interaction behaviour was to be modelled with the use of acoustic elements. The acoustic elements surround the plate structure in three sections. The first section is one element thick, and is responsible for the FSI-coupling (Fluid-220 elements). This means that the translation and pressure degrees of freedom of the innermost acoustic nodes are coupled to the translations of the solid elements of the plate. The translations result in a pressure, that then propagates through to the second fluid section (Fluid-30 elements). The second fluid section only describes pressure. The third, and outermost fluid section is a spherical boundary that emulates having an infinite fluid domain (Fluid-130 elements). The layout of the three types of acoustic elements can be seen in Figures 16a, 16b and 16c.

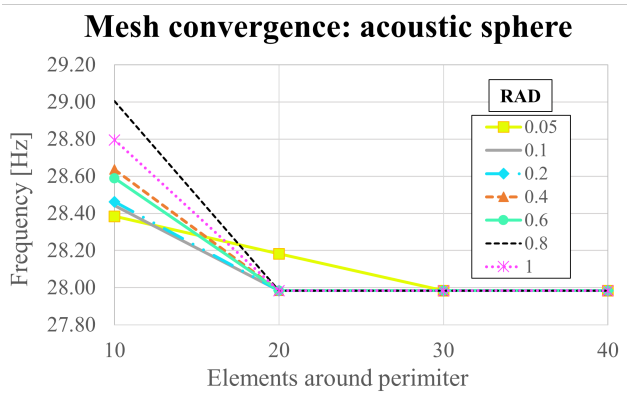

Figure 15: *Convergence plot showing frequency depending on number of elements around the sphere perimeter. The frequency to number of elements around the perimeter is plotted for different sphere radii. RAD=0.2λ ≈ 10.7 [m]*

To be able to resolve the pressure wave propagation in the fluid, it is recommended to use a sphere radius of 0.2λ, where $\lambda = \frac{c}{\omega}$ (ANSYS, 2023). Another recommendation is that there should be at least 6 elements within the wavelength of the highest frequency that is evaluated, in the solid and fluid domain

Since the plate behaviour is the thing of interest for this project, the fluid behaviour is only relevant to the degree of it affecting the structural behaviour. The behaviour of the plate was not necessarily changed, to a noticeable degree, if the pressure wave in the acoustic fluid could not be properly resolved. To investigate this, a convergence study of the acoustic mesh, was conducted.

The first step of the fluid mesh convergence study was to investigate the effect of refining the first layer mesh. The first layer mesh is dependent on the plate mesh, for compatibility reasons. This means that to refine the first layers mesh, the plate mesh must be refined. To determine whether or not improving the first layers mesh had a significant effect on frequency, the aspect ratio and number of element layers in the plate was increased. The differences were proved to be negligible, and the element size corresponding to an aspect ratio of 0.3 and 3 layers in the thickness was kept.

The second step of the fluid mesh convergence study was to investigate the effect of varying the sphere-radius and number of elements along the circumference. The second fluid layer, containing fluid-30 elements, was meshed with tetrahedral expansion from the smaller element size of the first fluid layer, to the larger element size at the spherical border. In Figure 17a, the accuracy of different discretizations for the of the first mode of vibration is tabulated for different radii and number of elements along the circumference (100% corresponds

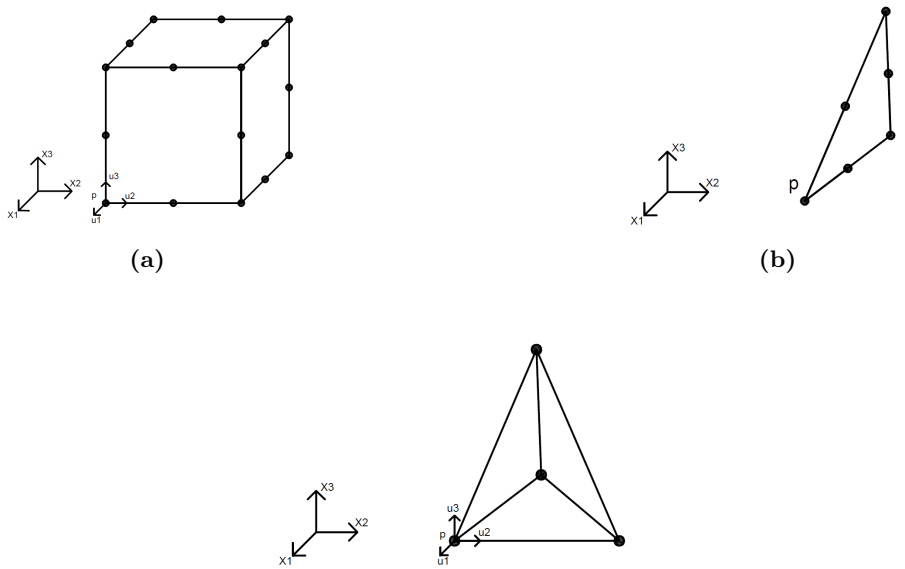

Figure 16: ***a)*** *Acoustic finite element with 20 nodes and 4 degrees of freedom per node. Three dimensional translation, and pressure. (Fluid-220),* ***b)*** *Acoustic finite element with 6 nodes and 1 degree of freedom per node. Only describes pressure on spherical boundary. (Fluid-130),* ***c)*** *Acoustic finite element with 4 nodes with 4 degrees of freedom per node. Three dimensional translation, and pressure. (Fluid-30).*

to the frequency of the finest mesh) The final mesh chosen for running the analyses can be seen in Figure 17b.

	0.05 RAD	0.1RAD	0.2 RAD	0.4 RAD	0.6 RAD	0.8 RAD	1 RAD
10	101.4%	101.6%	101.7%	102.3%	102.2%	103.6%	102.9%
20	100.7%	100.0%	100.0%	100.0%	100.0%	100.0%	100.0%
30	100.0%	100.0%	100.0%	100.0%	100.0%	100.0%	100.0%
40	100.0%	100.0%	100.0%	100.0%	100.0%	100.0%	100.0%

(a)

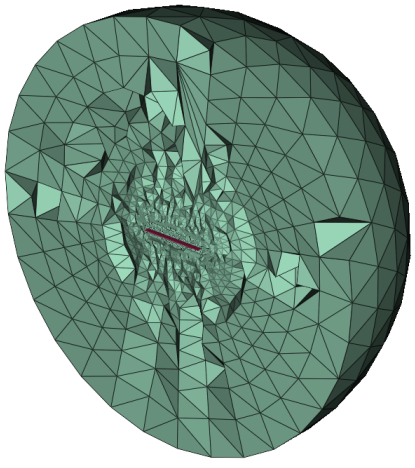

(b)

Figure 17: ***a)*** *Table with frequency values, normalized against the frequency obtained from the finest mesh tested (sphere radius = 1 RAD, elements around perimeter = 40). The columns represent different radii, and the rows represent the number of elements around the sphere perimeter.,* ***b)*** *Cross section of the acoustic discretization chosen for producing results.*

4.1.3 CFD-discretization

When developing the FSI-model, the solid FE-mesh from previous models was used for the plate. The fluid domain was modelled as a cube with a side length of 2 [m]. The mesh refinement inside the cube was set to increase when the distance to the plate became smaller. The element base-size within the cube was set to 0.01 m. The volume closer to the plate contained elements approximately one tenth of the base size. Adjacent to the plate, 5 prism layers were modelled. The prism layer mesh served the purpose of capturing the fluid boundary layer close to the plate surface. An illustration of the prism layers can be seen in Figure 19a.

Due to time limitations, a full CFD-mesh convergence study could not be conducted. The FSI-model required considerable computational resources and was also time consuming. An initial mesh refinement was chosen, and a simulation was run. Since the interaction between the plate and fluid is largely pressure dominated, the mesh was evaluated based on whether or not the pressure field could be properly resolved. In Figures 18a and 18b, examples of a badly resolved, and a well resolved pressure fields are shown. The parametric study of incompressibility also played a role in how the final mesh was chosen. In Figure 19b, the mesh used to produce results can be seen.

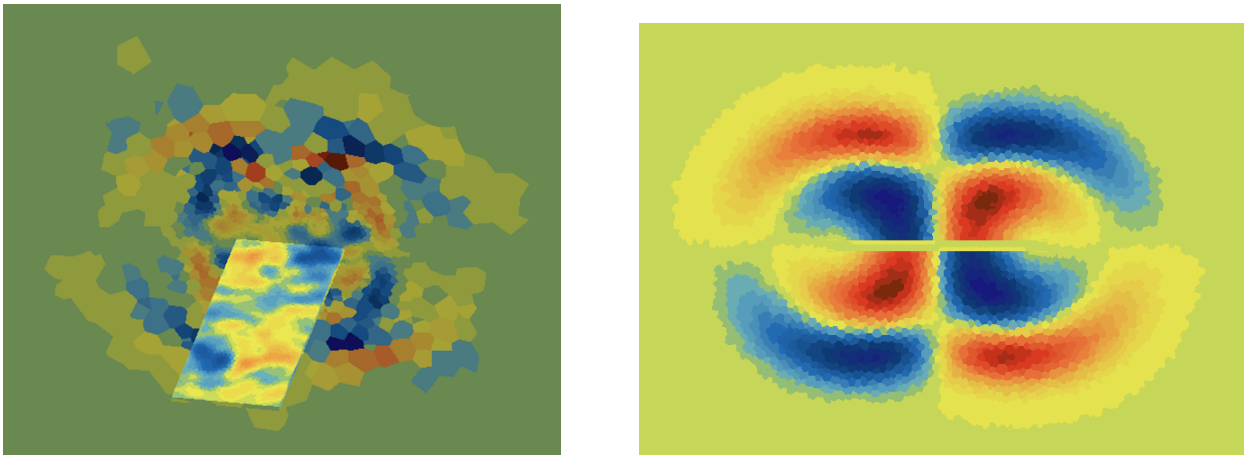

(a) **(b)**

Figure 18: ***a)*** *Badly resolved pressure field of second torsional mode,* ***b)*** *Well resolved pressure field of first torsional mode.*

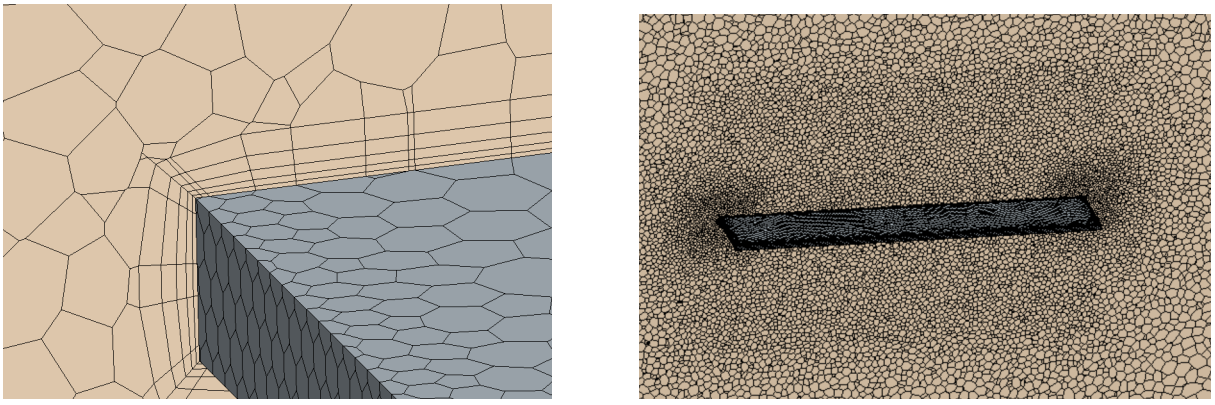

(a) **(b)**

Figure 19: ***a)*** *Illustration of prism layers closest to the plate surface,* ***b)*** *CFD mesh used for producing results.*

The final mesh chosen for producing results was also used in the parametric study of incompressibiliy. The lower modes of vibration did not require as fine discretizations as the higher modes. As the shape-complexity and frequency increased, the model required a finer time step and finer discretization to produce a stable response. Mode 1 required less computational power compared to mode 3. However, to eliminate the risk of inconsistent results due to a different mesh, the finest mesh, required for mode 3, was used to produce results for lower modes as well.

4.2 Parametric study of incompressibility

To obtain a stable response from the FSI model the incompressibility of the fluid was relaxed. This was done using field functions for the density and density gradient. The density ρ_F and density derivative $\dot{\rho}_F$ are defined by Equations (66) and (67). The speed of sound of an incompressible fluid is, in theory, infinite. The actual speed of sound in water is approximately, 1500 m/s. Setting the speed of sound parameter to, 1500 m/s in the field functions described above resulted in numerical difficulties. To get a stable result, the speed of sound was initially set to 50 m/s which is far from the actual physical value. To investigate how this effected the frequency and damping of the plate, a parametric study was conducted. The first, second and third mode of the simply supported, and the partially clamped plate was simulated with the same FSI-model, only changing the speed of sound. The results from the parametric study can be seen in Figures 20a-21b.

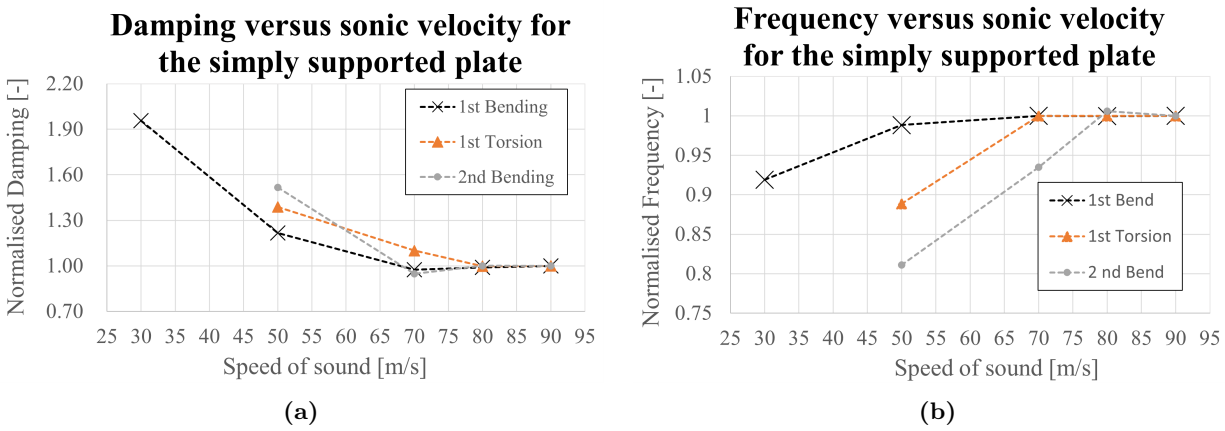

Figure 20: ***a)*** *Plot with damping results from the parametric study of the simply supported plate. The data has been normalized with respect to the damping obtained for the highest sonic velocity.,* ***b)*** *Plot with frequency results from the parametric study of the simply supported plate. The data has been normalized with respect to the frequency obtained for the highest sonic velocity.*

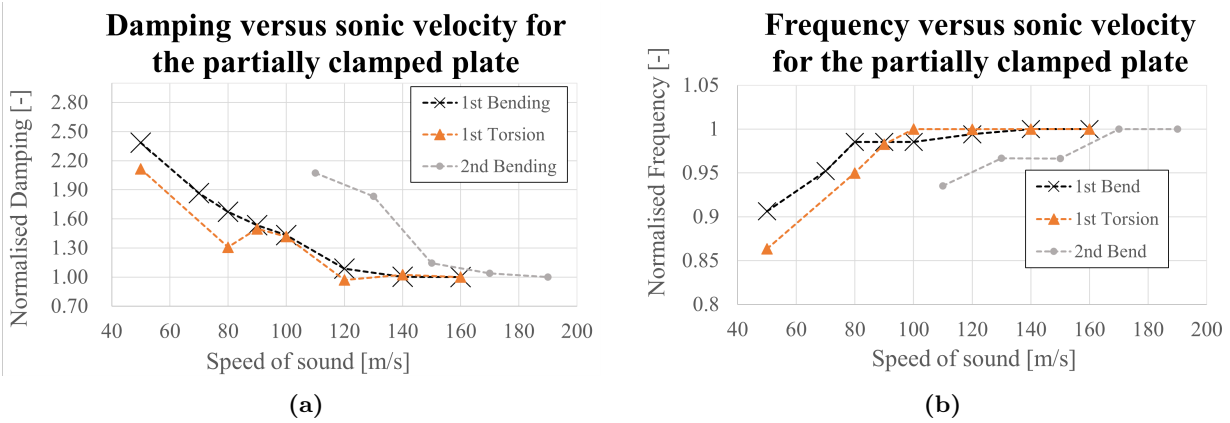

Figure 21: ***a)*** *Plot with damping results from the parametric study of the partially clamped plate. The data has been normalized with respect to the damping obtained for the highest sonic velocity,* ***b)*** *Plot with frequency results from the parametric study of the partially clamped plate. The data has been normalized with respect to the frequency obtained for the highest sonic velocity.*

The parametric study resulted in deeper understanding of how the incompressibility affects the damping and frequency. Within the sonic velocity range tested in this study, the damping and Frequency of modes 1-3

converged for increasing sonic velocities. The highest tested velocities for each mode respectively were chosen for producing the results. The velocities chosen for each mode are listed in Table 4. There is a possibility for the behaviour to change above or below the tested range, leaving some uncertainty in the results.

Table 4: *Sonic velocities chosen for producing results for mode 1-3 of both the partially clamped and the simply supported plate.*

Simply supported plate [m/s]	Partially clamped plate [m/s]	Mode
90	160	1st bending
90	190	2nd bending
90	160	1st torsion

4.3 Simply supported plate

In this section, results from the analysis of the simply supported plate are presented. The result data is tabulated and compared to experimental data for all modes. The transient and frequency response of some modes were left out of the report as they don't contribute to new information, besides the tabulated results.

4.3.1 AMAD model analysis results

The results from the AMAD analysis of the simply supported plate are presented in the figures and tables below. Table 5 contains frequency results for the first 5 modes of vibration in vacuum and in water. The results have been compared to experimental data in air and submerged and the deviation is also presented in the table below. The frequency was not assumed to differ a noticeable amount between air and vacuum, therefore the non-submerged, or vacuum-like, FE-results was compared directly to the experiment results in air. From the table data, one can see that the AMAD model performs better for bending modes compared to torsional modes.

Table 5: *Table with results from FE analysis of simply supported plate using the AMAD model.*

Mode	FE frequency without fluid effects[Hz]	FE frequency AMAD model [Hz]	Deviation from experiment in air [%]	Deviation from experiment submerged [%]
1	51.0	28.7	0.912	0.03
2	205.5	115.7	3.92	1.2
3	225.9	127.2	7.11	17.7
4	464.9	261.7	5.73	7.1
5	486.2	273.7	7.10	18.3

Figures 22a-22e are illustrations of the first five mode shapes of the simply supported plate. A scale factor was applied to the displacements to make the shapes more prominent in the images. The actual deformation used in the analysis was limited to a maximum of 10 mm. The transient response of the plate when excited in mode 1-5 can be seen in Figure 23. The frequency content of said modes can be seen in Figure 24. The transient response in this application refers to the time-displacement data of the node with maximum initial displacement in the plate. The frequency response refers to the fast Fourier transform of the time-displacement data of said node. The time displacement is in the shape of a decaying sinusoidal curve, which means that the plate moves with a damped harmonic oscillation. The damping comes solely from the manually applied Rayleigh damping according to design norms.

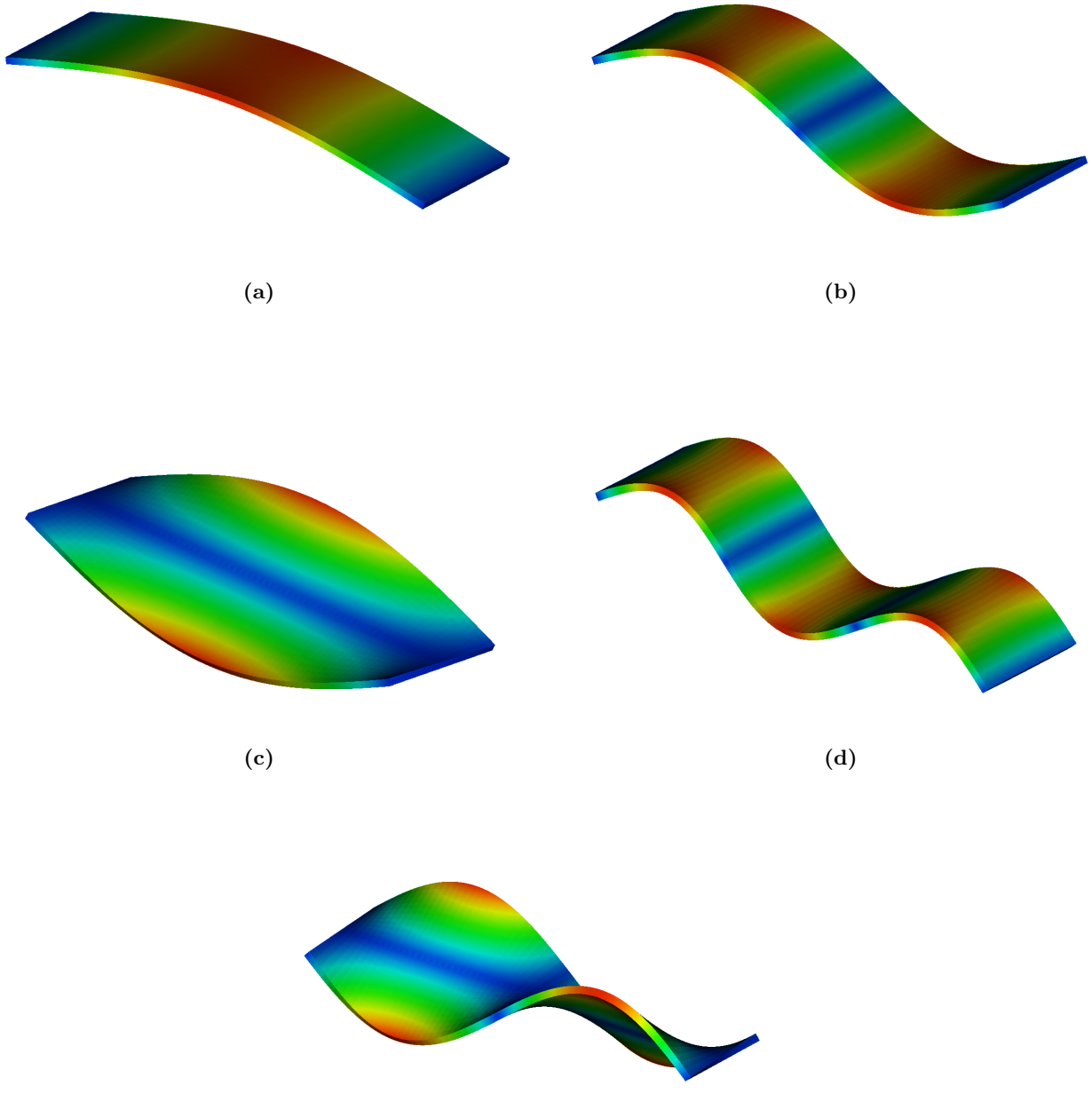

(a) **(b)**

(c) **(d)**

(e)

Figure 22: ***a)*** *(Mode 1) 1st Bending mode of simply supported plate.,* ***b)*** *(Mode 2) 2nd Bending mode of simply supported plate,* ***c)*** *(Mode 3) 1st torsional mode of simply supported plate,* ***d)*** *(Mode 4) 3rd Bending mode of simply supported plate,* ***e)*** *(Mode 5) 2nd Torsional mode of simply supported plate.*

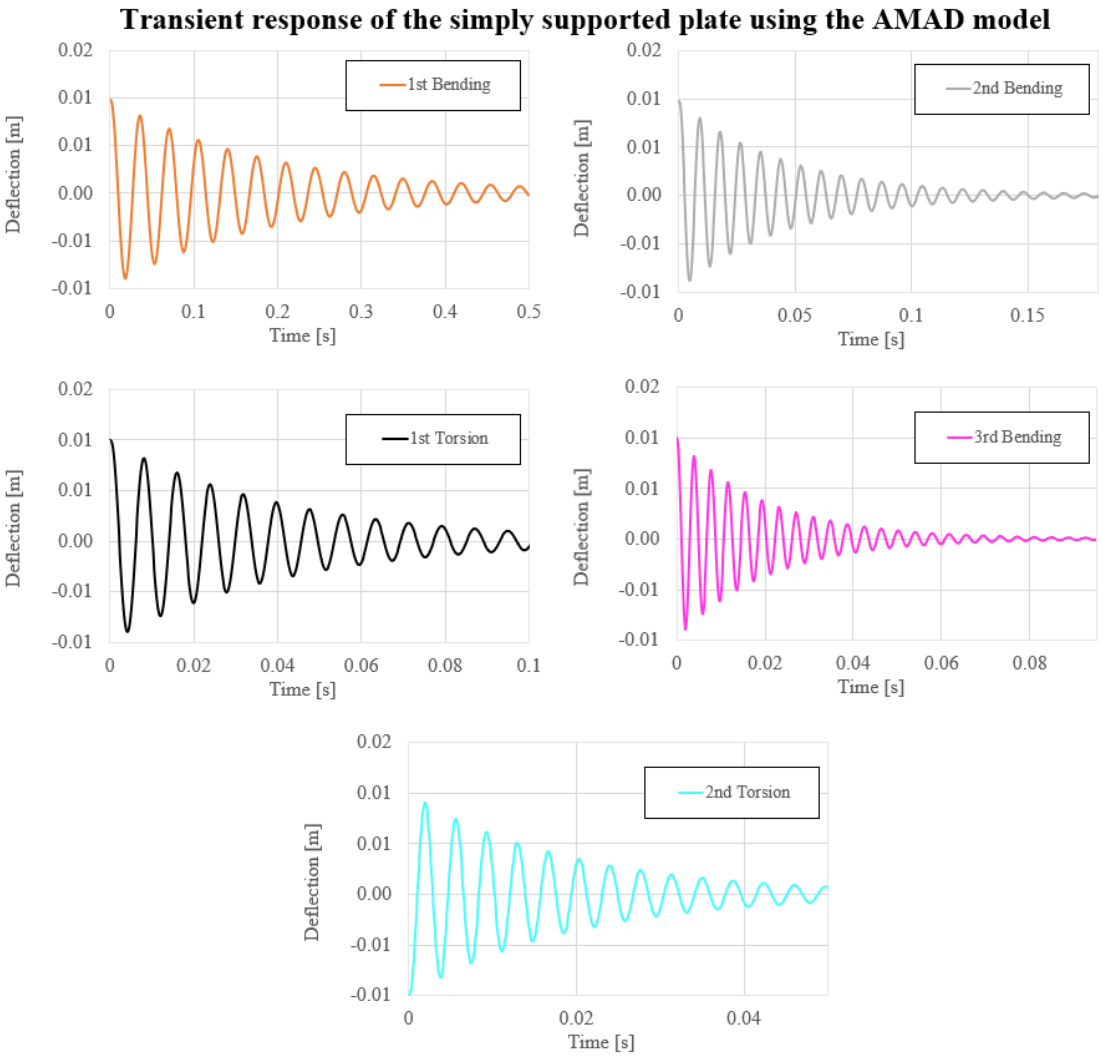

Figure 23: *Frequency content of the displacement data from the excitation of mode 1-5, using the AMAD model on the simply supported plate.*

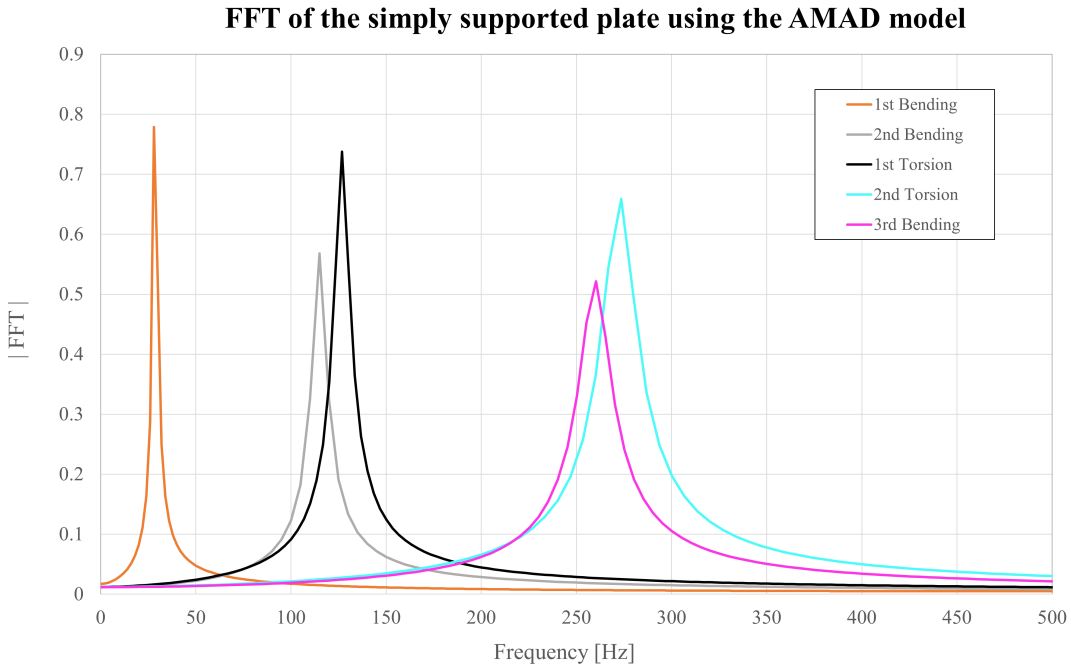

Figure 24: *Frequency content of the displacement data from the excitation of mode 1-5, using the AMAD model on the simply supported plate*

4.3.2 Acoustic element analysis results

Results from the analysis where acoustic elements are used to emulate fluid effects on the simply supported plate is presented in the figures and tables that follow. The frequency content of the displacement data from the excitation of mode 1-5 can be seen in Figure 25. Clear peaks can be seen in the frequency content, indicating a noise free response. The transient response of the acoustic model, and the undamped added mass model is compared in Figures 26a and 26b. The undamped response from the AMAD model was chosen for comparison as it illustrates the difference in frequency in a more clear fashion. The acoustic model did not show any signs of a damping effect. When comparing the response of the two plate models, when excited in the first bending mode, the response is similar. When doing the same comparison for mode 5, the same conclusion cannot be drawn. In Table 6, the eigenfrequency results of the first five modes from the acoustic analysis are presented. The deviation for the experiment conducted in water can also be seen in said table. From the results presented in this table, one can see that the deviation is substantially lower for torsional modes using the acoustic model compared to the AMAD model.

Table 6: *Table with results from the FE analysis of simply supported plate using the Acoustic model*

Mode	FE frequency Acoustic model [Hz]	Deviation from experiment in water [%]	Type
1	28.0	2.5	1st bending
2	120.5	2.9	2nd bending
3	156.6	1.1	1st torsional
4	285.7	1.4	3rd bending
5	329.5	1.7	2nd torsional

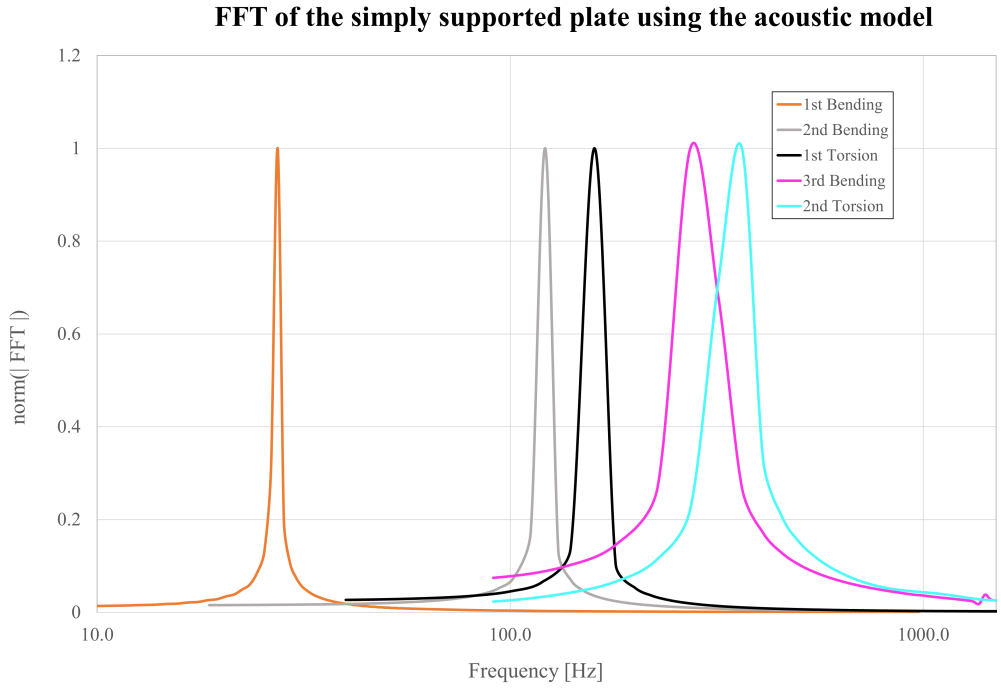

Figure 25: *Frequency content of the simply supported plate, excited in mode 1-5, using the Acoustic model. The y axis data has been normalized, and the x-axis is presented in log scale for illustration purposes.*

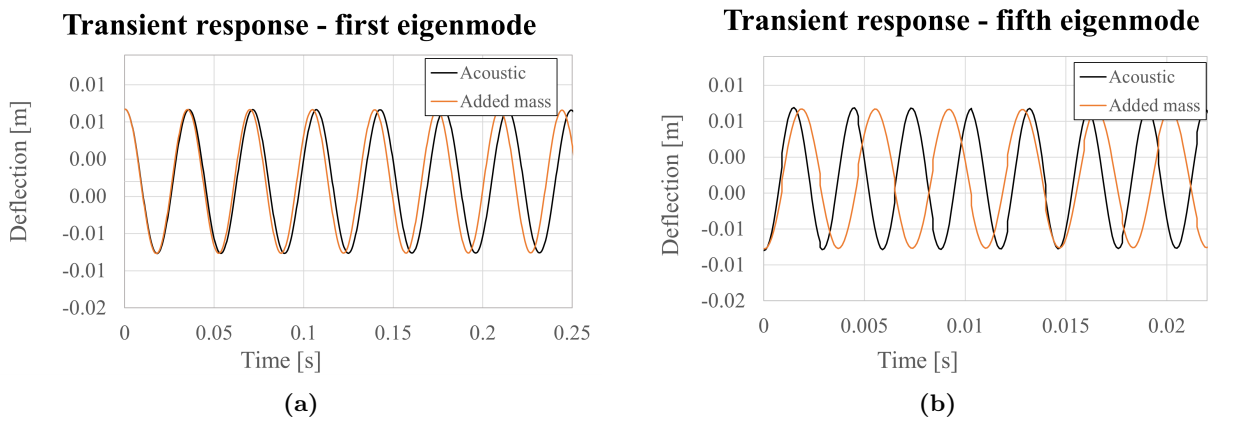

Figure 26: ***a)*** *Comparison between undamped response of AMAD model and the Acoustic model, vibrating in the 1st bending mode,* ***b)*** *Comparison between undamped response of AMAD model and the Acoustic model, vibrating in the 2nd torsional mode.*

The added mass factor for the five first modes was calculated using the frequency results from the non-submerged plate FE simulation and the frequency results from the acoustic analysis. The calculation was performed using the formula for added mass and frequency presented in Subsection 3.3. The added mass factors from the experiment, the acoustic model and the AMAD model are compared in Figure 27. One can see that the acoustic model does better overall, in estimating the added mass factor for higher modes of vibration, especially torsional modes.

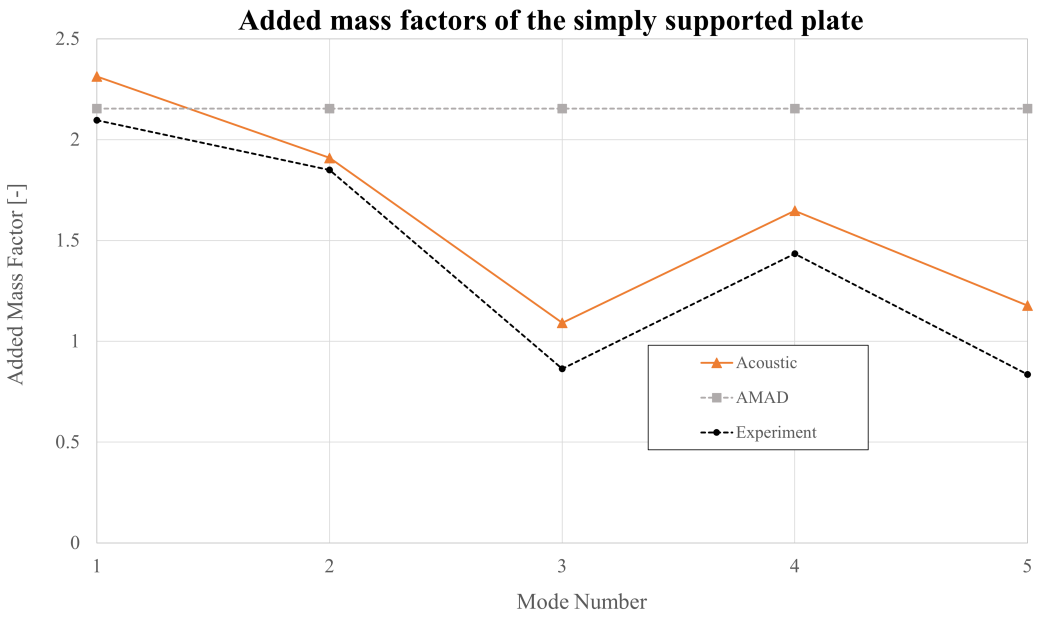

Figure 27: *Comparison of added mass factors of the simply supported plate for modes 1-5*

4.3.3 Full FSI analysis results

The results from the full FSI analysis of the simply supported plate are presented in this section. The frequencies of the first 3 modes are presented in Table 7 along with the deviation from the experimental results. Complete results for mode 4 and 5 was not produced. A more detailed explanation of this can be seen in Subsection 5.3. When looking at the deviation from experimental data for mode 1-3 using the FSI-model, one can see that a similar accuracy as the acoustic elements is obtained.

Table 7: *Table with frequency results from the FE analysis of simply supported plate using the FSI-model. [-] Indicates an unstable response*

Mode	Frequency FSI model [Hz]	Deviation from experiment in water [%]	Type
1	29.4	1.21	1st bending
2	116.9	0.14	2nd bending
3	156.3	1.13	1st torsional
4	-	-	3rd bending
5	-	-	2nd torsional

The model produced a damped transient response. The damping of each mode, given in percent of critical damping can be seen in Table 8. One can see that the damping is strongly dependent on mode shape when using the FSI-model.

Table 8: *Table with damping results from the FE analysis of simply supported plate using the FSI-model. [-] Indicates an unstable response*

Mode	Damping coefficient [%]	Type
1	2.51	1st bending
2	9.96	2nd bending
3	6.71	1st torsional
4	-	3rd bending
5	-	2nd torsional

The transient response, and frequency content from the excitation of the first three modes can be seen in Figures 28 and 29. The excitation of mode 1-3 gives, like the other models, a noise free, damped harmonic oscillation.

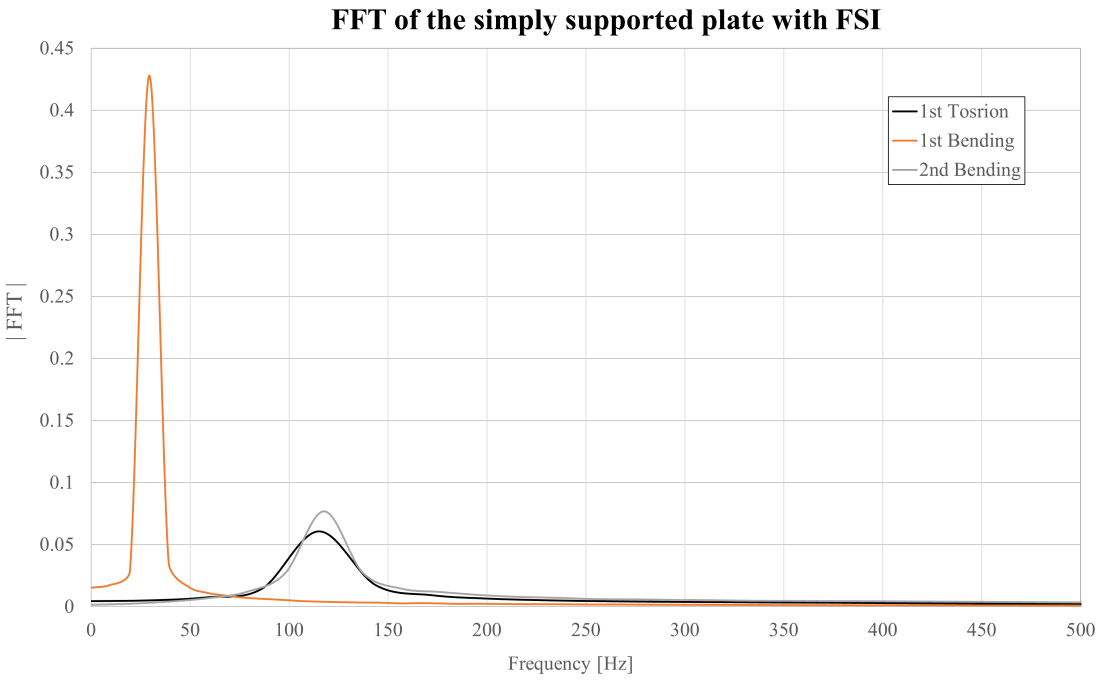

Figure 28: *Frequency content of the displacement data from excitation of mode 1-3 of the simply supported plate, using the FSI model*

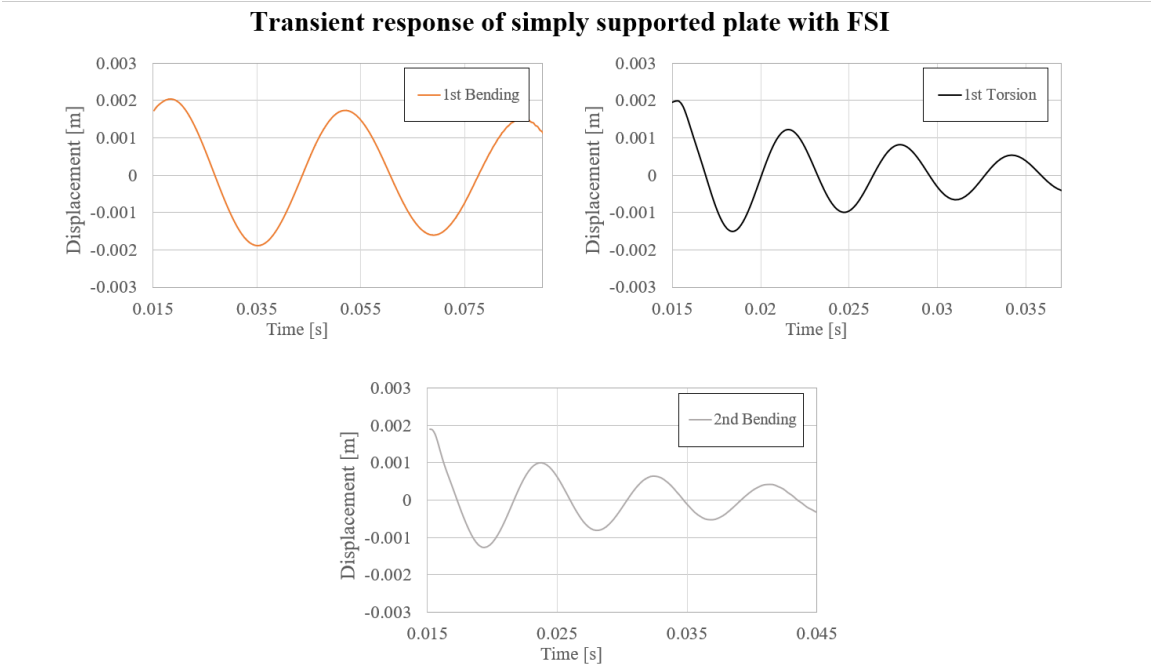

Figure 29: *Transient response of mode 1-3 of the simply supported plate, using the FSI model*

4.4 Partially clamped plate

In this subsection, results from the analysis of the partially clamped plate are presented. The result data is tabulated and compared to experimental data for all modes. The transient and frequency responses of certain modes were omitted from the report as they did not contribute any new information.

4.4.1 AMAD model analysis results

In the following figures and tables, the the results from the AMAD model analysis of the partially clamped plate are presented. The frequencies from the AMAD analysis can be seen in Table 10 for the first five modes. The frequency results from the non-submerged FE model can be seen in Table 9. The deviation from experimental data in air and submerged can also be found in said tables. One can see that, like in the case of the simply supported plate, the AMAD model does well when the first bending mode is excited. The model falls short when torsional modes are analysed.

Table 9: *Table with results from non-submerged FE analysis of partially clamped plate*

Mode	FE frequency without fluid effects [Hz]	Deviation from experiment in air [%]	Type
1	102.0	1.89	1st bending
2	238.8	2.34	1st torsional
3	283.7	1.65	2nd bending
4	509.8	1.41	2nd torsional
5	561.7	5.55	3rd bending

Table 10: *Table with results from FE analysis with AMAD of partially clamped plate*

Mode	FE frequency AMAD model [Hz]	Deviation from experiment in water [%]	Type
1	57.4	0.047	1st bending
2	134.5	24.95	1st torsional
3	159.7	4.36	2nd bending
4	287.02	25.59	2nd torsional
5	316.3	8.33	3rd bending

In Figure 30 the frequency response of the first five modes of vibration is plotted. The FFT:s give an indication of a clean transient responses, without noticeable excitation of unwanted modes.

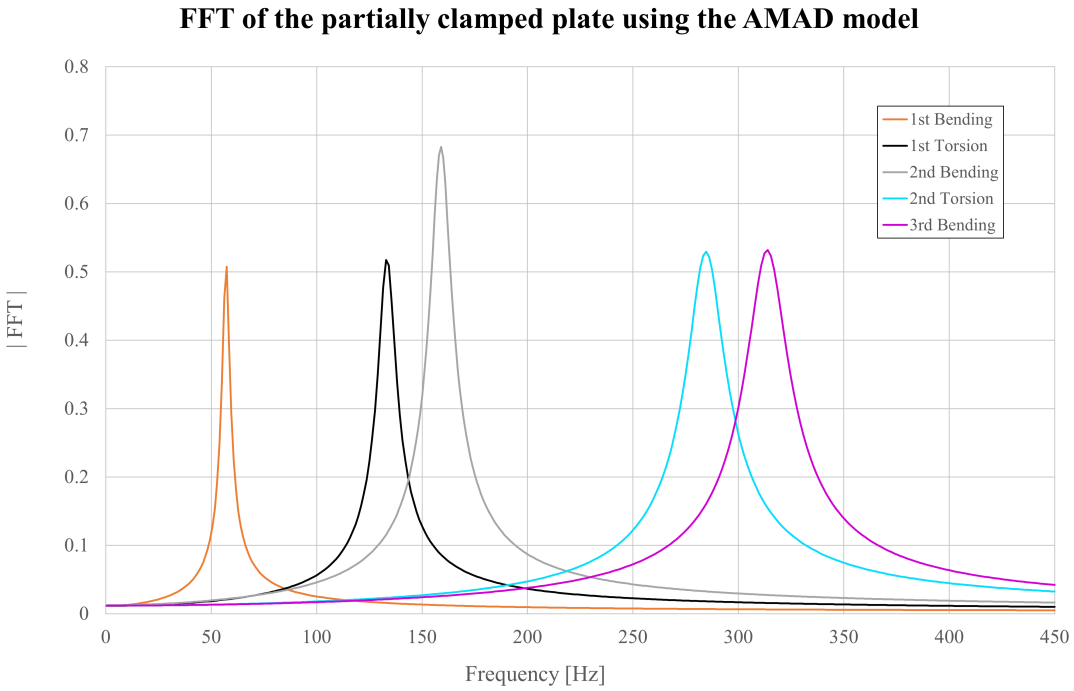

Figure 30: *Frequency content of displacement data, excitation of mode 1-5, added mass model, partially clamped plate*

In Figures 31a-31e, the mode shapes of the first five eigenmodes are illustrated. A scale factor was applied to the displacements of the modes for visual purposes. The actual displacement was, like for the simply supported plate, limited to a maximum of 10 mm. The transient response of mode 1-5 can be seen in Figure 32.

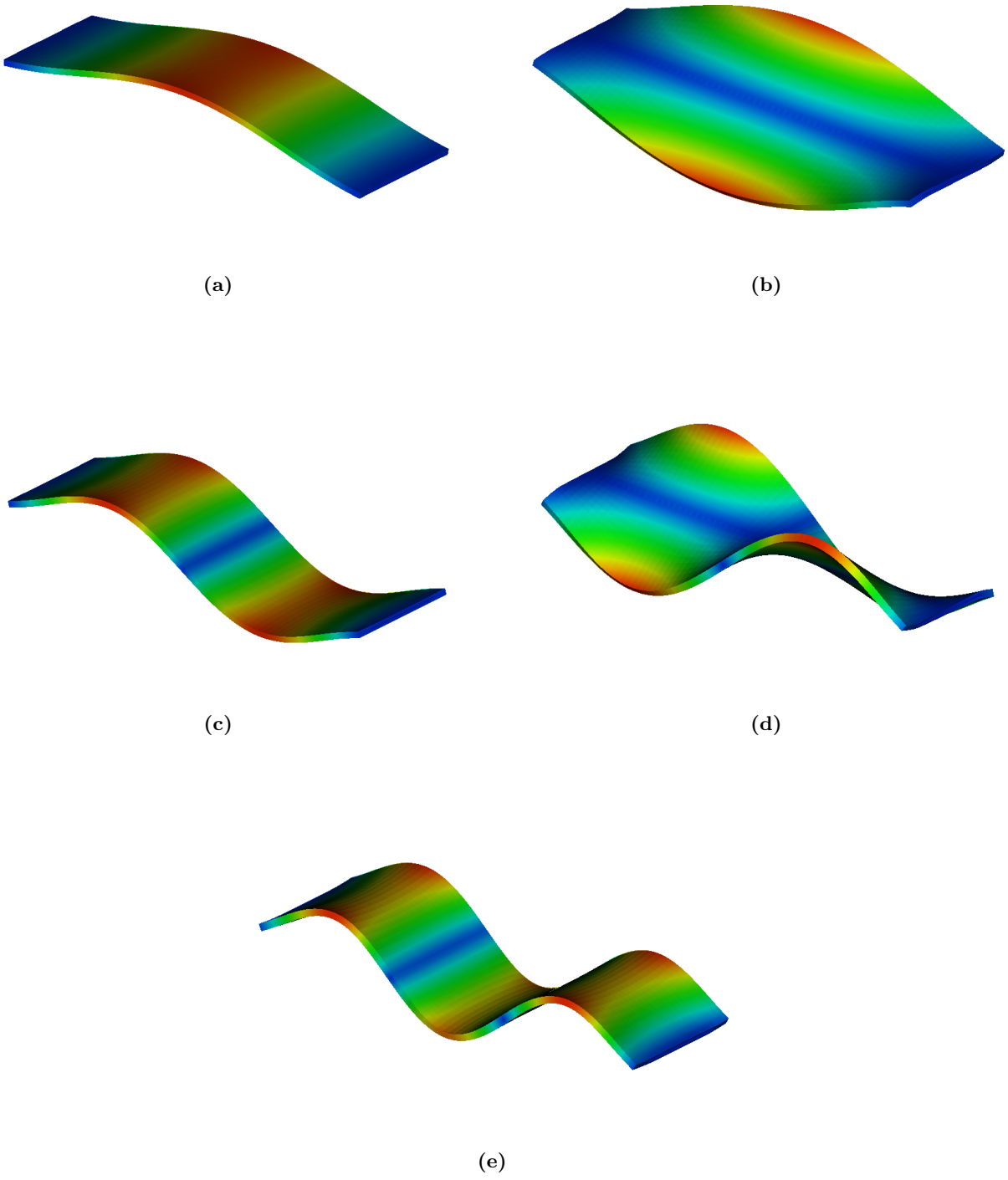

(a) **(b)**

(c) **(d)**

(e)

Figure 31: ***a)*** *(Mode 1) 1st Bending mode of the partially clamped plate,* ***b)*** *(Mode 2) 1st Torsional mode of the partially clamped plate,* ***c)*** *(Mode 3) 2nd Bending mode of the partially clamped plate,* ***d)*** *(Mode 4) 2nd Torsional mode of the partially clamped plate,* ***e)*** *(Mode 5) 3rd Torsional mode of the partially clamped plate.*

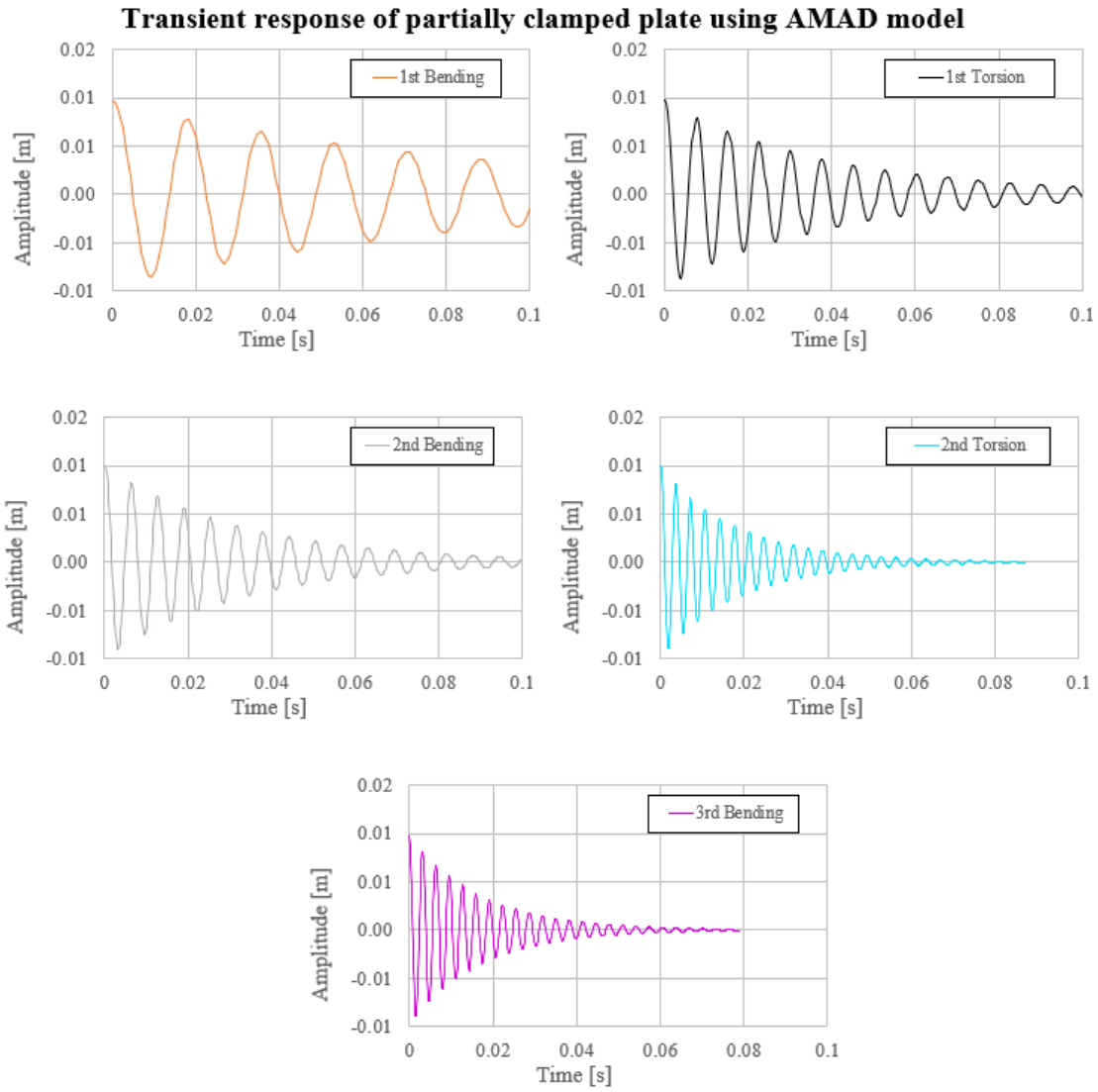

Figure 32: *Transient response of the partially clamped plate, when excited in mode 1-5, using the AMAD model.*

4.4.2 Acoustic element analysis results

In the following figures and tables, the results from the acoustic element model of the partially clamped plate is presented. The results from the frequency analysis, compared with the experimental data can be seen in Table 11. Like in the case of the simply supported plate, one can see that the acoustic model does better in determining the frequency of higher modes of vibration, compared to the AMAD model.

Table 11: *Table with results from FE analysis with acoustic elements of partially clamped plate in water.*

Mode	FE frequency Acoustic model [Hz]	Deviation from experiment in water [%]	Type
1	56.6	1.54	1st bending
2	166.7	4.36	1st torsional
3	167.3	0.1653	2nd bending
4	348.8	1.115	3rd bending
5	352.9	8.503	2nd torsional

Using the frequencies from the non-submerged FE-model analysis, and the frequencies from the acoustic model, the added mass factors were calculated for the five modes of vibration. The equation used for calculating the added mass factor can be seen in Subsection 3.4. The added mass of the plate remains constant for the AMAD model, regardless of mode shape. Like in the case of the simply supported plate, the acoustic model does a better job of estimating the added mass factors compared to the AMAD model, especially for torsional modes.

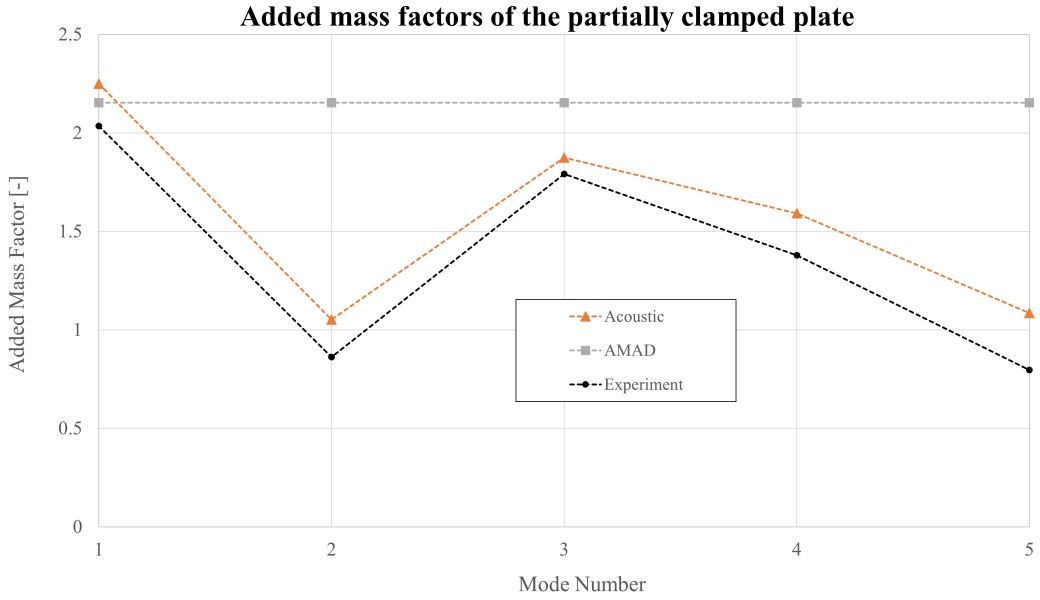

Figure 33: *Comparison of added mass factors of the partially clamped plate for mode 1-5.*

4.4.3 FSI analysis results

The procedure for analysing the partially clamped plate with full FSI coupling is the same as for the simply supported plate. The description for of the analysis method, FE and CFD models can be seen in Subsection 3.6. The only changes made to the model was the plate boundary conditions. The frequency results are compared with experimental data in Table 12. One can see that the FSI-model produces a similar accuracy as the Acoustic model with regards to eigenfrequency. Complete results for mode 4 and 5 was not produced. A more detailed explanation of this can be seen in Subsection 4.2.

Table 12: *Table with eigenfrequency results from FE analysis with full FSI of partially clamped plate in water. The initial amplitude was set to 0.002 m. [-] indicates an unstable response.*

Mode	FE frequency FSI model [Hz]	Deviation from experiment in water [%]	Type
1	59.0	2.71	1st bending
2	172.4	3.25	2nd bending
3	175.5	2.06	1st torsional
4	-	-	3rd bending
5	-	-	2nd torsional

Table 13: *Table with damping results from the analysis of the partially clamped plate using the FSI model with an initial amplitude of 0.002 m. [-] indicates an unstable response.*

Mode	Damping coefficient [%]	Type
1	3.57	1st bending
2	6.87	2nd bending
3	5.47	1st torsional
4	-	3rd bending
5	-	2nd torsional

The transient response of mode 1-3 can be seen in Figure 35. The frequency contents from the excitation of said modes can be seen in Figure 34. From these plots, it is evident that a clean response was obtained for the FSI-model analysis. Damped sinusoidal time-displacement curves, gave clean frequency contents.

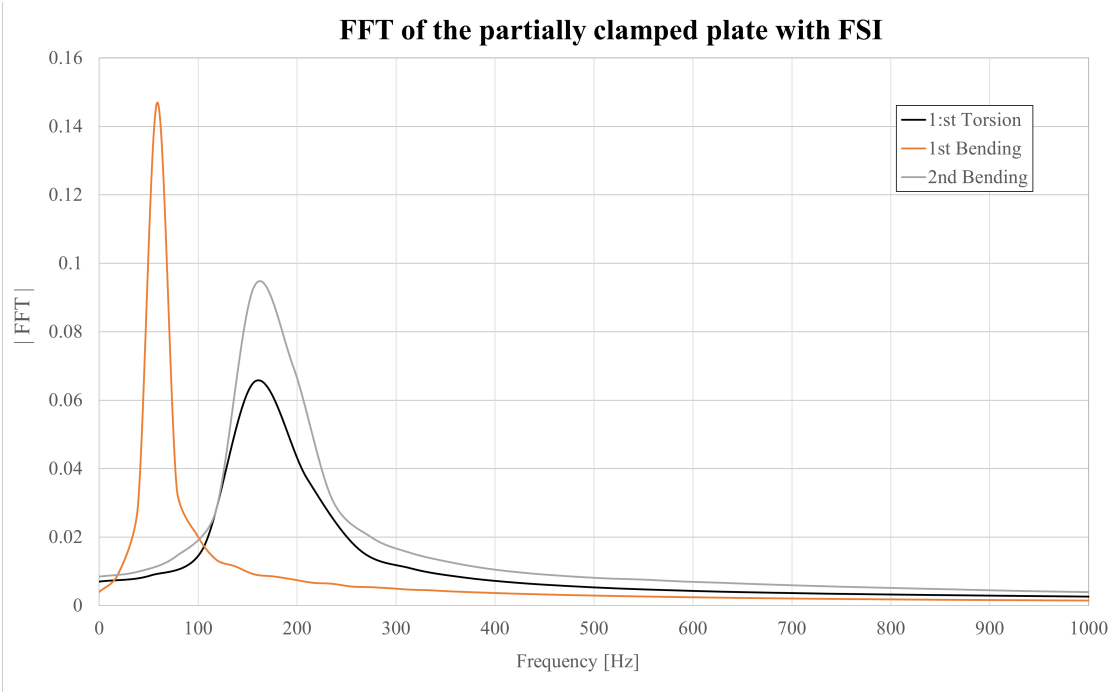

Figure 34: *Frequency content of the displacement data from excitation of modes 1-3 of the partially clamped plate, using the FSI model.*

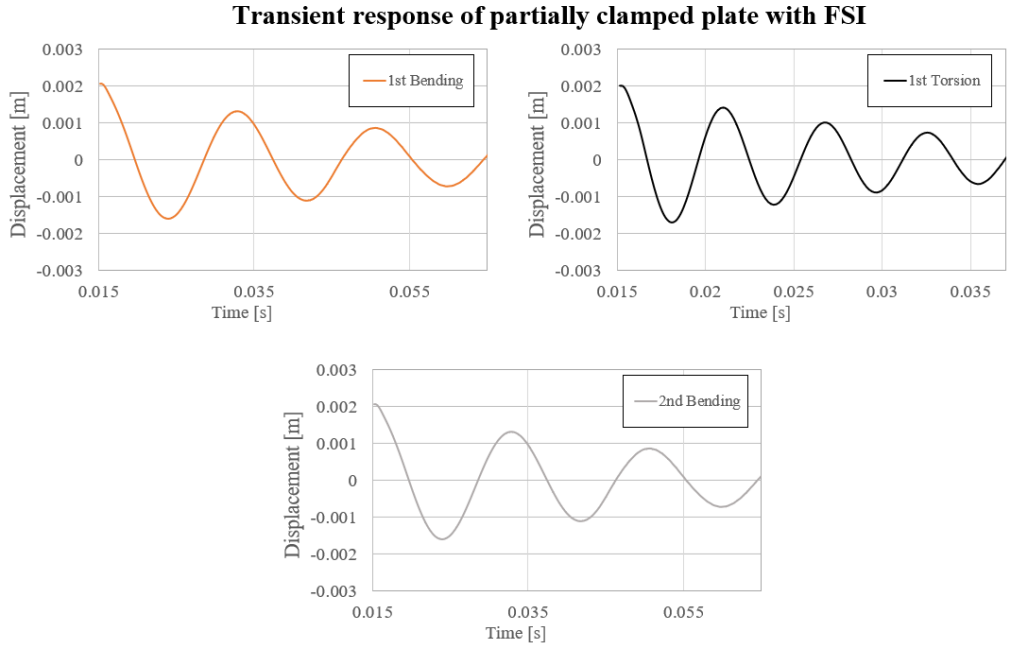

Figure 35: *Transient displacement data from the excitation of modes 1-3 of the partially clamped plate, using the FSI model*

5 Discussion

In this chapter, the results from the numerical implementation are discussed. The purpose is to gain an understanding of the advantages and shortcomings of the three modeling methods used.

5.1 AMAD model

The boundary conditions of the plates were not intuitive to set up, as one would assume that the notch-cut simply supported condition would be stiffer compared to an ordinary support where the plate is just supported on two edges. The experiment excited the plate via a rod placed in the middle of the plate. If the plate were to have only rested on top of two edges, the excitation would most likely result in the plate being lifted on and off the supports via the excitation rod. The plate needed to be held in place vertically without restricting it in rotation. This could have been done via some roller bearing-type fixtures at the edges. Friction would, however, occur, and to avoid this, the notch option was chosen instead.

When trying to emulate this boundary condition in the FE-plate, different configurations of restricted nodes were tested. This was also done to emulate the clamped boundary condition. When restricting nodes at the plate's shorter edges, node displacements in x, y, and z were locked. When testing out different configurations, the goal was to find a setup that resulted in the best fit to the experimental data, with regards to the eigenfrequencies in air. This was done manually, via trial and error. There was a great frequency sensitivity towards the boundary conditions, and to get an even better fit, a more thorough method could have been applied. To find the best combination of nodal restrictions, an optimization could be done, with the total frequency deviation set as the minimization objective.

The added mass assumption is based on rigid cross-sections translating in one direction in the fluid. For the bending modes of this plate, the cross-sections along the plate move in a manner that represents the assumption relatively well. The cross-sections also keep their shape relatively well in bending. In the case of torsion, the cross-section shapes are distorted and move in more directions than perpendicular to the plate's neutral axis. The added mass factor is strongly dependent on the mode shape for this type of geometry where the wavelength is comparable with the plate dimensions. This behavior cannot be covered by simply adding a fixed amount of mass.

5.2 Acoustic model

The plates that were analyzed fall under the category of geometries where the wavelength is comparable to the dimensions of the structure. In accordance with the theory presented by S.S Chen and Ho Chung, the added mass becomes dependent on the mode of vibration (S.S Chen & Ho Chung, 1976). This is not covered by the added mass model for 2D translation but is well-represented by the acoustic model in this analysis.

The FFT of the acoustic transient response gave a clear indication that the modal loading had only excited the modes of interest, which gave a negligible amount of interference or noise in the frequency content. This also confirmed that the mode shape deviates a negligible amount between air and water. The transient response of the acoustic model revealed a drawback related to damping. The acoustic elements gave a comparatively small damping factor, which was due to numerical loss, dependent on the time step and time integration method. This means that the acoustic elements do not contribute to any damping of the plate's movement. If one wants to implement damping effects on the plate, other options such as Rayleigh damping have to be applied with a reference percentage value, like in the AMAD model.

5.3 FSI model

To obtain a stable response from the CFD model, large computational resources are required. The movement of the plate in the coupled CFD and FEM system is governed by the pressure and wall shear stress exported from the CFD solver to the solid domain. The wall shear stress has a small magnitude compared to the pressure force from the fluid in this case. The pressure acting on the plate has proven to be hard to accurately

resolve, especially for higher modes of vibration. In the case of mode 1, which has a frequency of around 28 Hz and 57 Hz for the simply supported and partially clamped plates respectively, the pressure field could be resolved with a comparatively rough mesh size and time step.

To obtain a stable solution for modes 2 and 3, i.e., the first torsional and second bending mode, a more refined mesh was needed. For these higher frequency modes, the pressure waves became shorter and more complex. Numerical problems arise when there are too few elements within a wavelength, causing pressure gradients to increase. The transient response encounters interference early on in the simulation, and after only a few oscillations, the original mode shape is unrecognizable. Figures 36a and 36b illustrate the shape of the plate at 0.02 seconds (first oscillation) and at 0.18 seconds, respectively. Reliable results could not be obtained from this response and as the FFT was applied there where numerous amplitude peaks from 50 to 500 Hz.

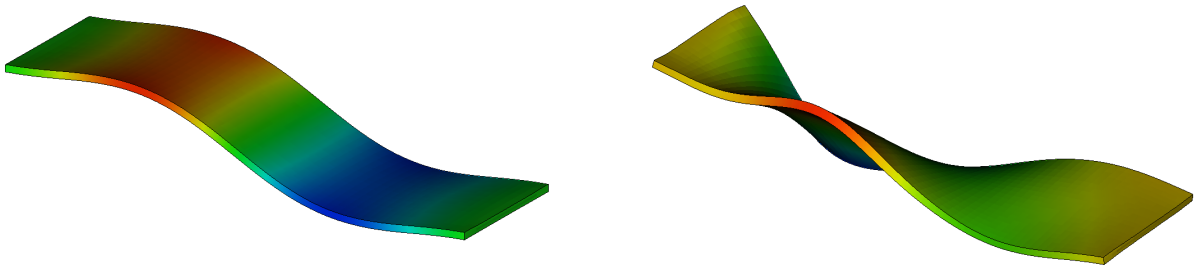

(a) **(b)**

Figure 36: ***a)*** *The shape of the partially clamped plate in the first oscillation of the unstable FSI-analysis of mode 3. A scale factor of 100 was applied to the plate for illustration purposes,* ***b)*** *The shape of the plate 0.18 seconds into the unstable FSI-analysis. A scale factor of 8000 was applied to the plate for illustration purposes.*

This sensitivity to meshing proved to be problematic in obtaining results. For consistency, the mesh used to produce results needed to be the same for all modes. Therefore, the mesh required for the highest mode analyzed was used to produce all results.

The fluid gives a considerable increase in damping in the FSI model. Experimental data, with absolute values, is needed to validate the model. Since the experiment conducted by M.R. Haddara and S. Cao only states the ratio between damping in air and damping in water, validation cannot be performed. FSI-simulations of the plate in air were performed in this project. The experimental data stated that a damping ratio of 3.14 for mode 1 of the simply supported plate, going from air to water. The FSI-damping in air for mode 1 was measured at 0.05%, and the damping in water was measured at 2.5%. Using a structural damping of 1% yields a ratio close to the experimental, 3.33%. However, the structural damping could be significantly lower or higher. The damping one can take into account according to norms is around 3%. Having that as a reference, the combined structural and fluid damping could be three or four times higher, depending on the mode.

The difficulty of applying higher sonic velocities is that smaller and smaller time steps and mesh sizes are needed to properly resolve the pressure waves. The possibilities of obtaining results for higher modes were investigated up to a mesh containing over 2.8 million elements, a time step of 0.05 milliseconds, and a sonic velocity of 250 m/s. When this failed, the computational cost of resolving mode 4 and 5 was deemed too high.

The incompressibility was, due to limitations in computational time, not investigated for sonic velocities

above 250 m/s, which is still far from the actual physical value of 1500 m/s. This raises questions about the relaxation and its impact on, amongst other things, interaction problems, where two adjacent structures are vibrating in fluid. The case of interaction could be a further development of this project.

6 Conclusion

This project has provided a detailed insight into different modeling techniques for submerged structures. Due to the limitations set on this project, there are still numerous unanswered questions about more complex geometries, interaction, numerical stability, flowing fluids, etc. Although there are many such unanswered questions, some conclusions can be drawn from the results produced in this thesis.

The AMAD concept was studied, both from a theoretical-analytical standpoint in the literature study and numerically using FE models. When analyzing the results from the FFT, one can conclude that the modal loading resulted in a noise-free response without noticeable excitation of the other modes. The eigenfrequencies of the bending modes deviated by up to 9%, with the first bending mode achieving accuracy within 1% for both the simply supported and partially clamped plate. Regarding the torsional modes, the accuracy declined, and the model gave eigenfrequencies that deviated upwards of 25%. This deviation is case specific and may vary with different geometries.

The AMAD model offers an undeniable advantage regarding computational cost compared to other methods. The fast computation time, combined with its relatively good accuracy in the first mode of vibration, explains why it is most commonly used in large-scale models in the industry. In practical applications of the added mass model, such as seismic analysis of submerged structures in nuclear power plants, the first mode of vibration is the most relevant. Through experimental data, it was found that the added mass factor of a structure is dependent on the mode shape. This behavior cannot be emulated by the AMAD model, where a constant mass is used across the frequency spectrum. To achieve this behavior, more complex models become relevant.

Acoustic element modeling was investigated as one of the alternatives to AMAD. The frequency was no longer lowered using a higher mass. Instead, a surface pressure, governed by the acceleration of the surface nodes, shared between fluid and solid, affected the plate's frequency. The acoustic elements were proved to be far more accurate than the AMAD model in determining the eigenfrequency of torsional modes. This, in addition to a relatively small increase in computational cost, gives a strong motivation to use acoustic elements. One major drawback of the acoustic elements is their inability to emulate structural damping. For this more complex behavior, an even more complex model is needed.

One can conclude that the model describes the frequency of the oscillatory motion more accurately than the AMAD model for torsional modes, and high order bending modes. The bending modes of the partially clamped plate are computed with less than 2% deviation from the experimental data, and the torsional modes are computed within 9%. The results from the simply supported plate remained within 3% for all modes. One can note that the simply supported plate results were more accurate for the acoustic model. However, the results without submersion were also more accurate for the simply supported plate to start with. The boundary conditions play a significant role in accurately determining the frequency, and the "clamped" boundary condition has proven to be harder to accurately model than the simply supported condition.

Full FSI modeling was investigated as an alternative and a "state of the art" modeling technique. When moving from acoustic elements to CFD-FEM coupling, the computational cost grew exponentially. On top of the computational cost, the time spent on setting up the model was significant compared to the other methods. High sensitivity to mesh, time step, domain size, and incompressibility required multiple iterations of the model-setup before results could be produced.

The frequency results from the full FSI model were not necessarily more accurate than the results from the

acoustic model. If one only cares about the frequency, the FSI model is not an effective way of determining it. The major advantage of the FSI model lies in its capability to simulate structural damping effects. Since the CFD-FEM coupled model is a "state of the art" modelling technique, it can be viewed as the closest thing to a experimental setup. It is possible to obtain damping results from the model, that are stable with regards to mesh and sonic velocity. If experimental data is not available, the FSI model could be used as an alternative. The use of damping levels determined by a FSI-model, in real world applications is not currently accepted. A recommendation for future work would be the investigate the capability of the FSI-model with regards to damping, and hopefully get approval to use it in design of nuclear components.

The sensitivity to incompressibility was significant. The frequency and damping converged to a relatively stable level when passing 70 m/s for mode 1 of the simply supported plate. However, this convergence threshold varied substantially between the different modes, ranging from 70 to 190 m/s. A trend of higher sonic velocities for higher modes of vibration gives an indication that mode 4 and 5 may require significantly greater speeds to produce reliable results.

Other applications where the FSI model can be justifiable to use lie beyond the scope of this thesis. The full benefits of using such a complex and computationally expensive model may not have come through in this simple application. Even though complex geometries have not been investigated in this thesis, the results give an indication of FSI and acoustic elements being able to more accurately determine the added mass and damping of such structures. Interaction problems and structures in a flowing fluid are examples of further developments in the analysis of submerged structures using FSI.

7 Further developments

In this chapter, analyses that build upon the results in the main project are presented. These analyses are presented with the purpose of sharing ideas on how the different methods investigated above can be used in other applications. Interaction problems and time signal analyses have been conducted.

7.1 Earthquake time-signal analysis

To substantiate the differences in the different modeling techniques, a practical application was performed. The goal was to investigate the difference in response between the AMAD and Acoustic models. This was done in the form of a time-signal response analysis. Two plates were modeled as cantilevers, with fixed supports at one end. Ground accelerations, generated from an earthquake response spectrum, were applied to the base over a time span of 15 seconds. Displacements at the free end and at the base were obtained. The ground acceleration data can be seen in Figure 37a. FFT was applied to the input signal to get an understanding of the frequency range.

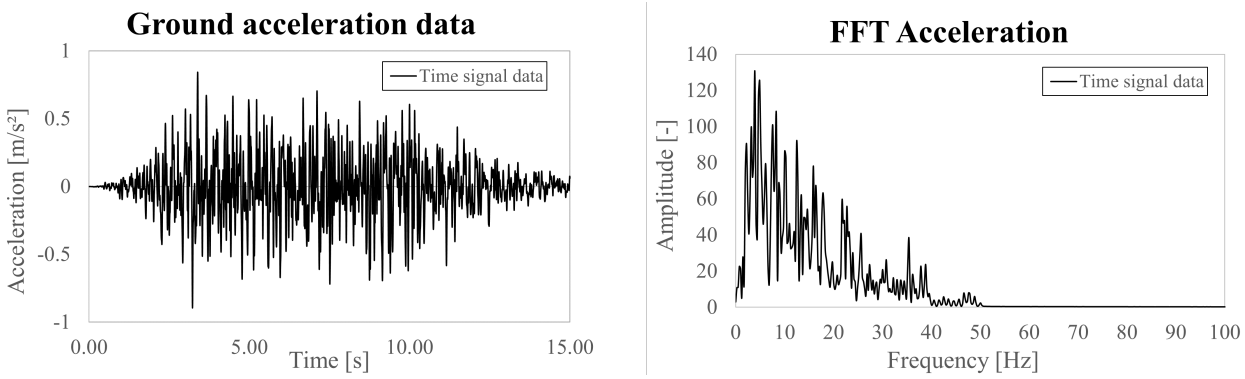

Figure 37: ***a)*** *Plot of the time signal data used as input for the analysis. The signal shows the ground acceleration during a 15 second time span,* ***b)*** *Plot of the fast Fourier transformed ground acceleration data. The main frequency contents lie within a span of 0-50 [Hz].*

First, a cantilevered steel plate with dimensions 9.36 x 201.65 x 655 mm was analyzed using both methods. For the acoustic model, the first eigenfrequency was measured at 10.77 Hz. The added mass model had a first eigenfrequency of 10.26 Hz. The displacement data from a node at the free end was analyzed with FFT, which gave a clear indication that the first eigenmode dominated the response in the ground acceleration analysis. The reason for only exciting the first mode is most likely that the input signal only contains a frequency range of 0-50 Hz. The second eigenmode has a frequency above 50 Hz for this plate, regardless of the model, which is beyond the input signal span.

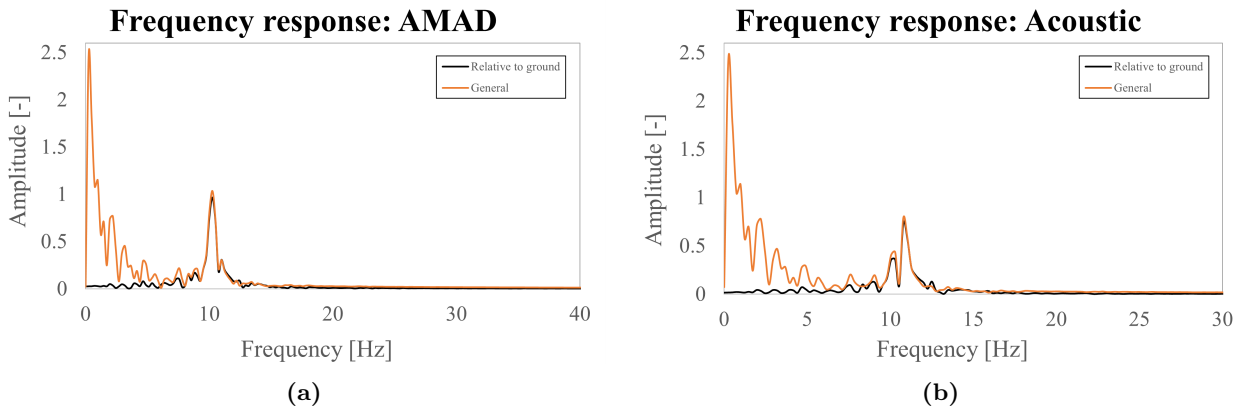

Figure 38: ***a)*** *FFT of the response at the unconstrained end of the plate, using the AMAD model,* ***b)*** *FFT of the response at the unconstrained end of the plate, using the acoustic model.*

When analyzing the displacement data from the two models, one could note that the maximum displacement was higher for the acoustic model. This would make the acoustic model a more conservative option when only looking at this response. To investigate this further, the sensitivity towards eigenfrequency was tested for the AMAD model. The added mass was determined using potential flow theory as in ASME norms and by using the frequency from the acoustic element analysis. This produced two plate models with a first eigenfrequency of 10.2 and 10.7 Hz respectively. The time signal analysis of these plates produced substantially varying responses. The difference in maximum displacement was 40%. With this in mind, one cannot give a conclusive answer as to which of the AMAD or Acoustic models is the least conservative. Having a slightly different structure or a slightly different input signal could drastically change the results in favor of either analysis method. With that said, all the time signal analyses conducted in this thesis yielded higher displacements for the acoustic model.

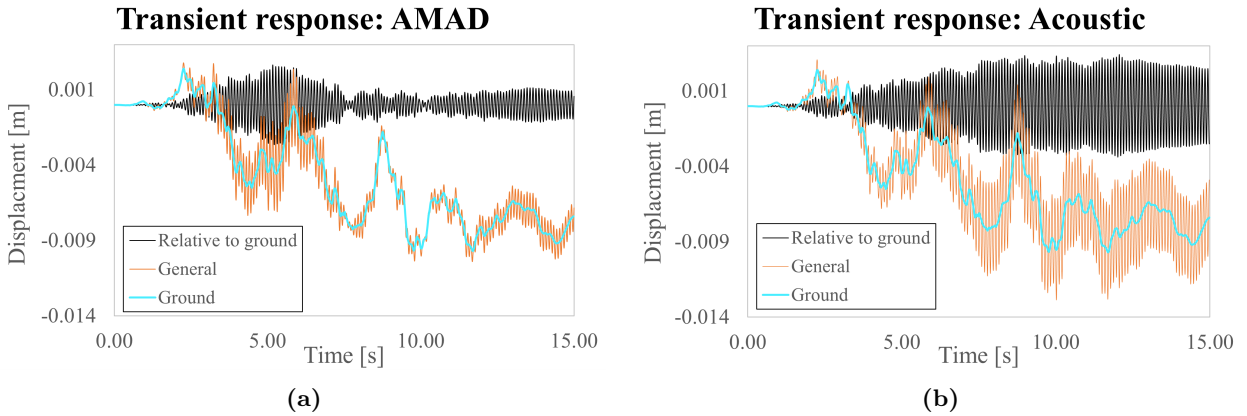

Figure 39: ***a)*** *Displacement data from the plate during the 15 second analysis time using the AMAD model. The ground displacement, the displacement at the free end, and the displacement at the free end relative to the ground is displayed in turquoise, orange and black respectively,* ***b)*** *Displacement data from the plate during the 15 second analysis time using the acoustic model. The ground displacement, the displacement at the free end, and the displacement at the free end relative to the ground is displayed in turquoise, orange and black respectively.*

The added mass and acoustic models of previous analyses produced similar frequency results for the first eigenmode, and this holds true for this time signal analysis as well. The differences in frequency estimation

started to diverge in previous analyses for higher-order modes. To observe if the same discrepancy manifested itself in the time signal response, a thinner plate was modeled. A plate with dimensions 4.36 x 201.65 x 655 mm was used. The second mode of the thinner plate fell within the frequency range of the input signal. The response of the thinner plate for the acoustic and added mass models can be seen in Figures 40a and 40b.

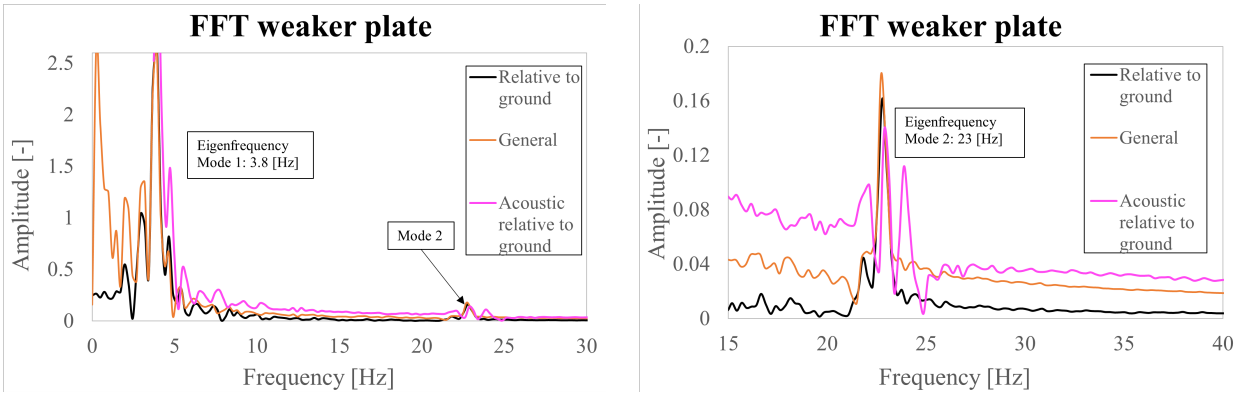

(a) **(b)**

Figure 40: ***a)*** *FFT of the response at the unconstrained end of the thinner plate, using the AMAD model,* ***b)*** *Zoom-in on mode 2 peak.*

The AMAD model predicts the second eigenfrequency within 1 Hz of the acoustic model. This is most likely due to the fact that the second eigenmode, like the first, is a bending mode, which the AMAD model has been relatively good at predicting.

7.2 Interaction

The AMAD model, as stated in norm calculations, does not take interaction into account. To investigate if and how the acoustic model reacts to interaction, a double plate model was set up. Two identical simply supported plates were analyzed with different C-C distances. The plates were set into free vibration using the same modal plucking method used in previous analyses. In-phase and out-of-phase vibrations were analyzed with respect to eigenfrequency. The shape of the plates before being released into free vibration in the transient analysis can be seen in Figures 41a and 42b.

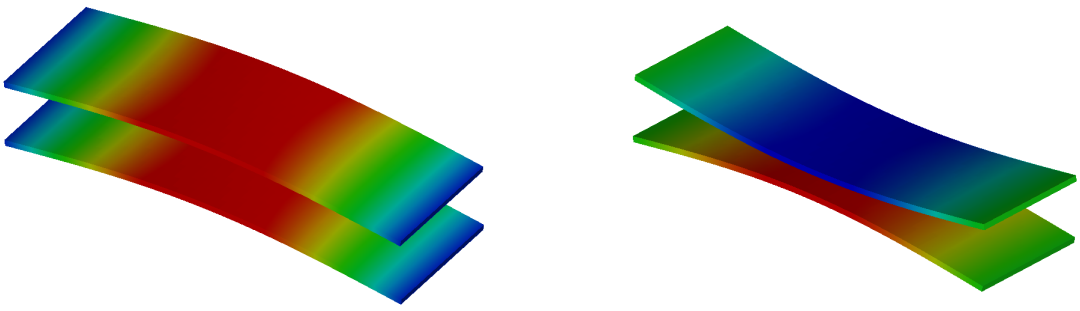

(a) **(b)**

Figure 41: ***a)*** *Initial shape of the double plates upon release. The plates are displaced in the same direction for in-phase oscillation,* ***b)*** *Initial shape of the double plates upon release. The plates are displaced in the same direction for out of-phase oscillation.*

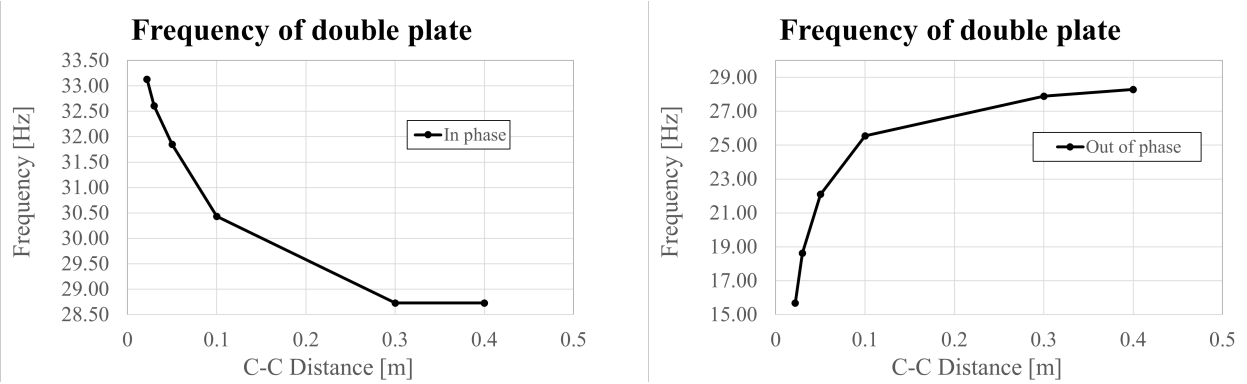

Figure 42: ***a)*** *Plot of the frequency depending on the C-C distance between the double plates oscillating in-phase,* ***b)*** *Plot of the frequency depending on the C-C distance between the double plates oscillating out of-phase.*

The results from this study confirms that the acoustic model can take interaction effects into account. To get an indication whether or not the observed behaviour of the acoustic model is reasonable, a benchmark study against the FSI-model could be conducted. However, due to time limitations, this was not a possibility.

References

Anderson, J. D. (2003). *Modern compressible flow*. McGraw-Hill.

ANSYS. (2023). *Elements for acoustic analysis*. Retrieved February 20, 2023, from https://www.mm.bme.hu/~gyebro/files/ans_help_v182/ans_elem/elem_acouselems.html

ASME. (2021). *Bpvc section iii-rules for construction of nuclear facility components-appendices*. Retrieved January 24, 2023, from https://www.asme.org/codes-standards/find-codes-standards/bpvc-section-iii-div-1-appendices/2021/print-book

Craig, R. R., & Kurdila, A. J. (2006). *Fundamentals of structural dynamics*. John Wiley Sons.

Datta, T. K. (2010). *Seismic analysis of structures*. John Wiley Sons (Asia) Pte Ltd.

Davidsson, P. (2004). *Structure-acoustic analysis; finite element modelling and reduction methods* (Doctoral dissertation). Lund University.

Epps, B. P. (2005). *2.016 hydrodynamics*. Retrieved January 24, 2023, from http://web.mit.edu/2.016/www/handouts/Added%5C%20Mass%5C%20Derivation%5C%20050916.pdf

M. R. Haddara & S. Cao. (1996). *A study of the dynamic response of submerged rectangular flat plates*. Memorial University of Newfoundland.

Ottosen, N., & Petersson, H. (1992). *Introduction to the finite element method*. Prentice hall.

Roger Y. Lu & David D. Seel. (2006). *Pwr fuel assembly damping characteristics*. Westinghouse Electric Co.

Siemens Digital Industries Software. (2023). Simcenter STAR-CCM+ User Guide, version 2021.1. Siemens. https://docs.sw.siemens.com/documentation/external/PL20200805113346338/en-US/userManual/userguide/html/STARCCMP/GUID-28A739CF-6DE2-4D87-B582-E390B522011C.html#

S.S Chen & Ho Chung. (1976). *Calculating hydrodynamic mass part i: Circular cylindrical structures*. ARGONNE NATIONAL LABORATORY.

Techet, P. A. (2005). *Potential flow theory*. Retrieved January 24, 2023, from https://web.mit.edu/2.016/www/handouts/2005Reading4.pdf

U.S. Nuclear Regulatory Commission. (2007). *Damping values for seismic design of nuclear power plants*.

W.R. Marcum, K. Britsch, P.L. Harmon, S. Liu, A. Weiss, T.K. Howard, & M. Moussaoui. (2019). *Numeric benchmark study of plate vibration experiments in air and water*. International Journal of Thermodynamics.

Y. Kerboua, A.A. Lakis, M. Thomas, & L. Marcouiller. (2007). *Vibration analysis of rectangular plates coupled with fluid*. E cole Polytechnique of Montre al,,Institut de Recherche d'Hydro Que bec.

CHALMERS